The Dissertation Committee for Greg Nate Holt
certifies that this is the approved version of the following dissertation:

Generalized Approach to Navigation of Spacecraft Formations Using Multiple Sensors

Committee:

E. Glenn Lightsey, Supervisor

Wallace Fowler

Michael Moreau

Cesar Ocampo

Byron Tapley

Generalized Approach to Navigation of Spacecraft Formations Using Multiple Sensors

by

Greg Nate Holt, B.S., M.S.E.

DISSERTATION

Presented to the Faculty of the Graduate School of

The University of Texas at Austin

in Partial Fulfillment

of the Requirements

for the Degree of

DOCTOR OF PHILOSOPHY

THE UNIVERSITY OF TEXAS AT AUSTIN

August 2006

To God from whom all blessings and wisdom flow,

To the dedication of one's life to the pursuit of wisdom,

To my wife's support through this long task,

To my parents for their devotion and example.

Acknowledgments

I would like to thank my advisor, Dr. E. Glenn Lightsey, for his enthusiastic support of my graduate studies and research. Thanks also goes to Dr. Oliver Montenbruck for his work with the Orion GPS receiver that was used as part of this study. Many humble thanks also go to my committee for time and consideration even amongst their busy schedules.

A special acknowledgement is given to my student colleagues for their lively discussion and debate. Thanks to Jacob Williams for encouragement and good humor through many long hours in the GPS Lab. Thanks to Tom Campbell, Jamin Greenbaum, Tena Wang, Jeff Mauldin, Shaun Stewart, and all the other devoted members of the FASTRAC nanosatellite team at the University of Texas for their collaboration on an exciting spaceflight project.

Generalized Approach to Navigation of Spacecraft Formations Using Multiple Sensors

Publication No. ____________________

Greg Nate Holt, Ph.D.
The University of Texas at Austin, 2006

Supervisor: E. Glenn Lightsey

An investigation was performed to evaluate sensor suitability and performance for formation flying in a variety of spaceborne environments. This was done as a precursor to the development of strategies for novel uses of satellite formations in environments other than Low Earth Orbit. Sensor models were developed to allow for a uniform treatment in processing range measurements. A formation simulation environment was then produced which included representative formation geometries, sensor noises, and navigation filters. The simulated formations included Low-Earth, highly elliptical, and libration point orbits. Equations of motion were modified to account for more accurate propagation of elliptical orbits, and an estimator was designed that allowed for large propagation times without GPS measurements. A high-accuracy transponder measurement was added and evaluated to give improved performance to accuracies of a few meters. A similar study was performed for the libration point orbit without the capability to track GPS signals.

Table of Contents

List of Tables

List of Figures

Chapter 1

Introduction

1.1 Background

Satellite formation flying is an emerging technique for making detailed scientific observations, monitoring the space environment, and performing co-operative satellite projects. Mission concepts such as TechSat21 [14] and Orion/Emerald [26], though never flown, paved the way for the field of co-operative satellite operations. Several missions have flown as of this writing, including EO-1 / LandSat7 [6], GRACE [43], CLUSTER II/Phoenix [18], ST5 [35], and FORMOSAT-3/COSMIC [47]. In addition, several missions are in the planning stages, including Magnetospheric Multiscale Mission(MMS) [13] and ST9 [29]. All of these missions have prescribed relative position and attitude requirements that are tailored to their requirements. Many of these missions have utilized the terrestrial Global Positioning System (GPS) constellation as a primary method of relative position navigation. The basic technology for this system has been present since the early 1980s, but only recently has it been utilized for real-time relative navigation. Some early missions used this method with extensive ground support [31]. There are, however, a host of other sensors that can be utilized to good effect when navigating formations of satellites, both in relative positioning and attitude determination. The choice of these depends upon the orbit environment of the formation and the requirements of its particular mission. Additional sensors may include one-way RF, two-way RF, optical ranging, magnetometers, and gyroscopic sensors to name a few.

Measurement models are not new to the field of navigation, and are in fact essential to filter design and estimation problems. High fidelity measurement models are useful for simulating the performance of a sensor and evaluating its suitability for a particular application. In the field of spacecraft formation flying, the existing measurement models primarily deal with the Global Positioning System and other 1-way, time of flight radionavigation sensors.

1.2 Motivation

With such varied applications and sensor choices, mission designers may have trouble determining which sensor or sensor suite will meet the requirements appropriate to their specific mission. What is needed, and what this dissertation seeks to present, is a uniform and quantifiable approach to sensor selection for formation flying missions.

A recent example of this need was demonstrated with the FASTRAC (Formation Autonomy Spacecraft with Thrust, Relnav, Attitude, and Crosslink) mission. This student-built nanosatellite from The University of Texas was seeking to perform attitude determination using GPS signal-to-noise ratio measurements from a single uniform-gain antenna. This attitude solution, however, was indeterminate in the direction of the GPS antenna boresight. Additional sensor measurements were needed, and this helped motivate the development of the generalized techniques shown in this dissertation. In the case of FASTRAC, these measurements were provided a magnetometer.

Satellite formations research has driven the development of lower cost, more capable, and more robust space missions. A preponderance of this research, however, has focused on applications for medium or low altitude Earth orbits (LEO). For these missions the dominant navigation sensor proposed is the Global Positioning System (GPS). The benefits of satellite formations, however, are not limited to the immediate vicinity of Earth and can be extended to many other space missions, including platforms at libration point and interplanetary orbits. Spacecraft formations of this variety, however, will spend the majority of their operational lifetime with limited access to the GPS navigation signal. This research, therefore, also seeks to evaluate the suitability and efficacy of additional sensors for use on these missions.

A generalized approach for modelling sensor ranging measurements in a positioning algorithm, therefore, is needed. These models would be used to generate measurements for complex mission simulations. Navigation filter performance can be evaluated and tuned in these simulations before more expensive hardware testing is commenced. A generalized ranging model also allows simple modification of individual noise sources, satisfying the need to examine the effects of a particular source on the navigation performance. This can lead to recommendations about the best methods to improve overall mission performance by suppressing the most significant error sources.

1.3 Literature Review

Much of the literature relating to relative navigation of spacecraft formations can be broken into four categories: requirements definitions, sensor analysis, relnav testbeds, and current/proposed missions.

The classic requirements definition documents for generalized satellite formation flying are from Bauer and Leitner. Bauer, et. al. describe a host of missions that require varying levels of formation flying accuracy [5]. This paper also surveys the state of relative navigation sensors and testing environments. Leitner lays out the expected performance needs of formation flying missions in the near and long term [29].

Sensor analysis has been recognized as an important step in the development of satellite formation flying. Stewart and Holt [40] describe the preliminary development of an all-purpose GPS sensor for absolute navigation, relative navigation, and attitude determination. How and Tillerson [24],[44] have analyzed sensor noise from a control viewpoint, noting that for representative LEO formations the fuel usage can increase linearly with signal degradation. Corrazini [12] suggest using one-way RF measurements to augment CDGPS when signal availability is limited or missing. Alonso, et. al. [2],[1] describe an optical system for spacecraft relative navigation using LED beacons. Simulation results are presented showing accurate relative ranging and attitude determination. Robertson, et. al. [39] describe another optical system that is coupled with differential GPS. Yim, et. al. [48] even theorize an optical doppler system for interplanetary spacecraft, presenting an entirely new measurement type. The Autonomous Formation-Flying (AFF) sensor as described by Purcell, et. al. [38], Aung, et. al. [3] and Lau [28] has been developed and prototyped at NASA's Jet Propulsion Laboratory (JPL). It is a dual one-way ranging system using Ka-band carrier and several coding and metrology methods for precise relative positioning. It is a candidate to fly on the Terrestrial Planet Finder and Micro-Arcsecond Xray Imaging Mission.

Formation flying testbeds have also been developed and documented. Naasz, et. al. describe a hardware-in-the-loop testbed for formation flight algorithms used at GSFC [36]. Algorithms such as those described in Busse, et. al. [10] utilize this testbed for performance evaluation. Ebinuma [16] demonstrates precision spacecraft rendezvous using GPS relative navigation. As part of the study, a GPS software simulation was used for evaluation of the relative filter performance and sensitivity to receiver dependent errors such as integer ambiguity and receiver clock errors. Ferguson, et. al. [20], describe a system-level testbed for evaluating formation flying architectures with all hardware components in the loop.

Several studies have also been done on current and proposed satellite formation missions. Moreau, et. al. [34] demonstrated flight results from GPS used in a HEO mission aboard the AO-40 amateur radio satellite. Gill, et. al. [22], describe a technology demonstration mission for GPS relative navigation. Ferguson and How [19] describe estimation architectures for formations of satellites in various scenarios including MEO, GEO, and beyond. Folta, et. al. [21] describe a representative mission, the MAXIM libration orbiter. This consists of a swarm of spacecraft distributed approximately 1 km about a hub. Moreau, et. al. describe several current and proposed HEO missions that utilize GPS [33]. They produced a HEO GPS simulation and demonstrated results for representative missions.

1.4 Contributions

This dissertation makes several contributions to the field of satellite formation flying.

1.4.1 LEO Microsatellite Sensor Development

As part of this research, a LEO formation flying sensor was theorized, developed, tested, and implemented aboard a spacecraft. This involved extensive modification and reworking of the attitude determination algorithm into an orbit reference frame and aboard a dual-antenna spacecraft. There were also numerous issues addressed with regard to microprocessor memory and embedded hardware delays to take the experimental simulation to an actual flight-ready sensor. The finalized sensor has been included in the Formation Autonomy Spacecraft with Thrust, Relnav, Attitude and Crosslink (FASTRAC) mission planned for launch in late 2006 or 2007 [40]. This is the first time that a single sensor capable of GPS positioning, real-time on orbit relative navigation, and attitude determination has flown aboard a spacecraft.

1.4.2 Sensor Measurement Models

This dissertation presents a generalized approach to modelling range measurements in a relative positioning algorithm. The advantages to this approach are twofold. First, scenario simulations can easily be adapted to incorporate single or multiple sensors for relative navigation. Second, results from these scenarios can be confidently compared since the underlying range measurement equations use common error models. A new formulation of the two-way radionavigation problem is presented as an example.

1.4.3 Error Characterization

An important contribution of this research is the definition of high fidelity ranging equations for formation flying sensors. These formulations are used in the sensor models and demonstrated in simulation with representative estimation techniques for various formation flying scenarios. These quantifiable error measurements allow mission designers to adopt a uniform approach for comparing and selecting formation sensors for different missions.

1.4.4 HEO/Libration Orbit RelNav Filters

For formations in HEO, where absolute references such as GPS may have outages, a sample relnav estimator is designed which accounts for these outages and expected disturbances. In addition, the equations of motion in this estimator are tailored for more accurate HEO propagation. Similarly, a sample relnav filter is presented for a formation in a Libration orbit where external measurements are very rare. All of these scenarios can be accurately compared because the underlying measurements used by the filters come from the generalized ranging models described earlier.

1.4.5 Sensor Fusion

A demonstration is given for appending new measurement types to an existing filter to perform sensor fusion. The example shown is for two-way ranging, but could be extended to other sensor types perhaps not yet defined or even invented.

1.4.6 Applications

This dissertation demonstrates the application of various measurement types to specific formation problems, including Low Earth Orbit, High Earth Orbit, and Libration Point missions as examples of how the results can be applied to many different formation flying mission studies.

1.5 Overview of Dissertation

The following chapters present the details of the generalized approach to modelling range measurements in a positioning algorithm. Chapter 2 begins with an overview of the radionavigation process and then presents the generalized ranging measurement equations. Approaches for both one-way and two-way ranging are addressed. Chapter 3 describes the development of flight hardware for a LEO formation mission and uses the previously described measurement equations in a LEO simulation. These simulation results are used to verify the measurement models used in the next chapter. The fourth chapter, then, extends these measurement models and simulations into a HEO environment. Representative versions of GPS-only, transponder-only, and combined sensor filters are presented and demonstrated. Chapter 5 extends the study to the case of a formation of libration point orbiters. Again, a representative navigation filter is presented and demonstrated. Finally, chapter six summarizes the contributions made during the course of this study and also presents ideas for follow-on research.

Chapter 2

Radionavigation Overview

Radionavigation is the science of determining position, velocity, attitude, and other state information based on the measurement of electromagnetic (radio) waves. For more details about the physics of electromagnetic waves, see Misra [32] or Hofmann-Wellenhoff [23].

2.1 Time of Flight

The time of flight sensor methodology involves measuring the time taken by a transmitted signal while travelling a defined path. Multiplying the signal propagation time by the speed of light gives the path length and range. This may be accomplished by utilizing one-way or two-way signals.

2.1.1 Signal Paths

Figures 2.1 and 2.2 show the signal paths that are used in one-way and two-way ranging, respecetively. One-way time of flight ranging is perhaps best known as the fundamental measurement of the U.S. Global Positioning System (GPS) [25]. It can, however, be used in other radionavigation schemes as well. A transmitter sends a signal at start time t_s and it is received at end

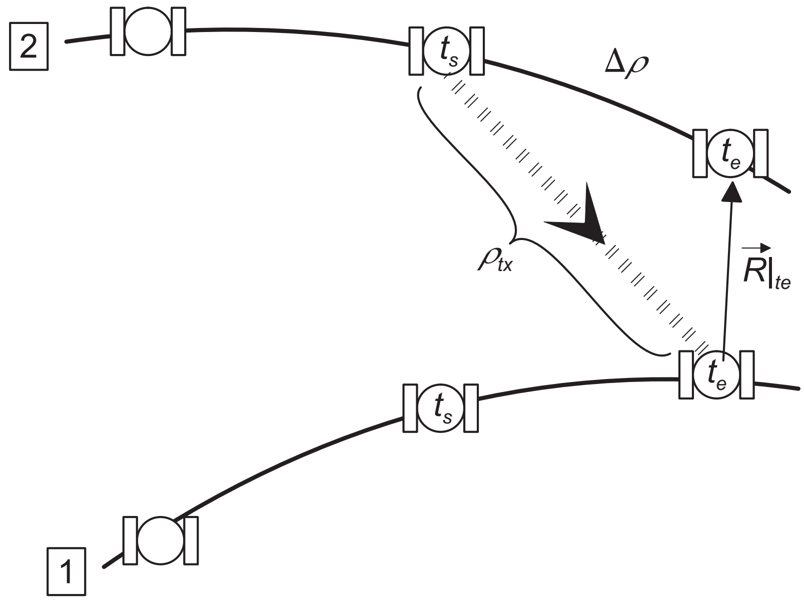

Figure 2.1: 1-Way RF Measurement Diagram

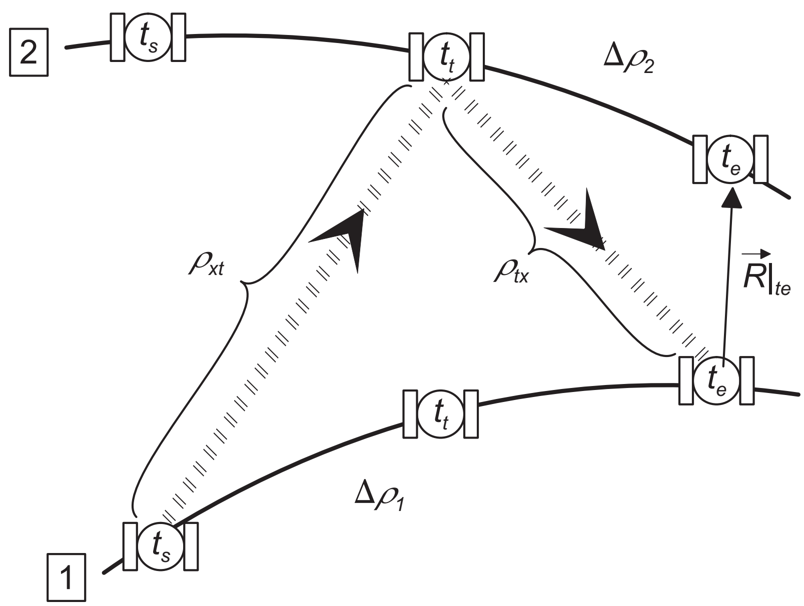

Figure 2.2: 2-Way RF Measurement Diagram

time t_e. During that interval the transmitter has moved to a final relative position $\vec{R}\,|_{te}$. The projection of that change along the line-of-sight is denoted by $\Delta\rho$. If multiple transmitters at known locations are used, the receiver can determine its position.

In two-way time of flight ranging, the fundamental measurement is accomplished by noting the time it takes for a transmitted signal to reach a transponder, undergo retransmission, and travel back to the original sender. The transceiver sends a signal at start time t_s, it is received and rebroadcast by a transponder at time t_t, and is finally received by the transceiver at end time t_e. During the entire interval the transceiver has changed position, and the projection of that change along the line-of-sight is $\Delta\rho_1$. During the return trip interval the transponder has moved by a projected amount $\Delta\rho_2$. Once multiple transponder measurements are taken, the sender can determine its position.

2.1.2 Mathematical Representation

Measuring time-of-flight of a radio signal generally involves a phase measurement from either a generated code or the carrier wave itself. Both the transmitter and receiver will perform their operations using internal clocks, and any discrepancy between these clocks and an overall "system time" will cause a measurement bias. Typically, this bias is estimated along with the vehicle state in the navigation filter. The measurement itself, commonly referred to as the *pseudorange*, is the combination of the geometric range, the overall clock bias, and any other modelled or unmodelled error sources. Figures 2.3 and 2.4 graphically show the development of the time of flight measurements. It is notable that the one-way measurement contains contributions from both the transmitter and receiver clocks, while the two-way measurement only has components from the transceiver clock. The one-way time of flight measurement is shown in Equation 2.1. This formulation is well defined in GPS literature such as Misra [32] and Kaplan [25].

$$
\begin{aligned}
& && \text{One-Way Geometric Range,} \\
R\,|_{te} &=&& c(t_e - t_s) + \Delta\rho \\
& && \text{One-Way Pseudorange,} \\
\rho &=&& c\left[(t_e + \psi\,|_{te}) - (t_s + \zeta\,|_{ts})\right] \\
& && +\Delta\rho + c\Delta_{tx} + c\Delta_{xr} + \nu \\
&=&& c(t_e - t_s) + c(\psi\,|_{te} - \zeta\,|_{ts}) \\
& && +c\Delta_{tx} + c\Delta_{xr} + \nu \\
&=&& R\,|_{te} + c\delta t + c(\Delta_{tx} + \Delta_{xr}) + \nu
\end{aligned}
\tag{2.1}
$$

where

$$
\begin{aligned}
t_s &= \text{System time at which the signal left the transmitter} \\
t_e &= \text{System time at which the signal reached the user receiver} \\
\zeta\,|_{ts} &= \zeta(t_s) = \text{Transmitter clock state at } t_s \\
\psi\,|_{te} &= \psi(t_e) = \text{Receiver clock state at } t_e \\
\delta t &= \zeta\,|_{ts} + \psi\,|_{te} = \text{Overall clock bias contribution}
\end{aligned}
$$

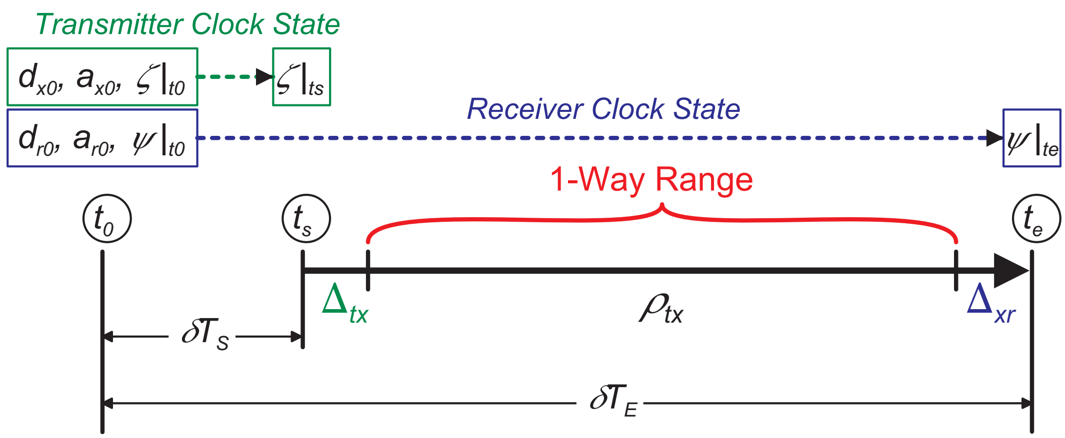

Figure 2.3: 1-Way Time of Flight Measurements

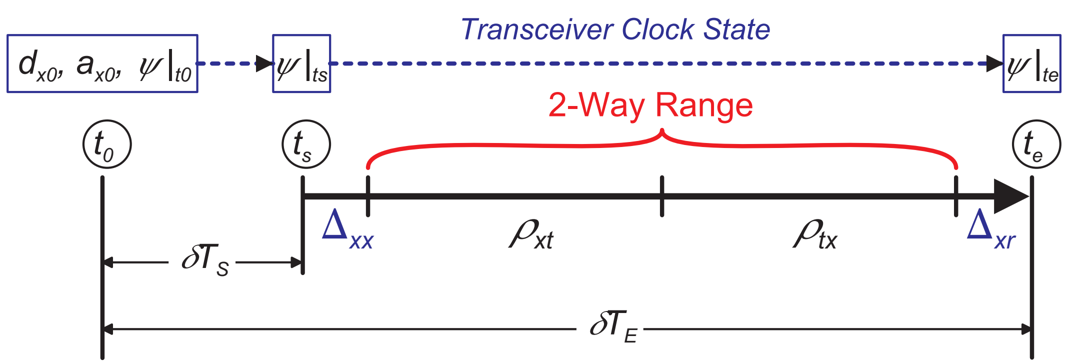

Figure 2.4: 2-Way Time of Flight Measurements

$$
\begin{aligned}
R\,|_{t_e} &= \text{True scalar range at signal receipt (end)} \\
\Delta\rho &= \text{Change in position of transmitter during time-of-flight} \\
& \text{projected along the line-of-sight direction} \\
\Delta_{tx} &= \text{Transmitter line delay} \\
\Delta_{xr} &= \text{Receiver line delay} \\
c &= \text{Speed of light} \\
\nu &= \text{Unmodelled error contributions}
\end{aligned}
$$

The two-way time of flight measurement is shown mathematically in Equation 2.2. This has been used previously in ground tracking systems such as the NASA Deep Space Network (DSN) [7]. It has not been used extensively, however, for relative navigation of spacecraft formations. Since it does not have the heritage of a well-studied relative navigation system such as GPS, it is not as well defined in the literature as the one-way measurement. The two-way time of flight measurement is presented here in a parallel formulation to the one-way time of flight measurement as a demonstration of how ranging measurements from new sensors can be expressed in an easily comparable form. This formulation also facilitates incorporation of the additional sensor into existing navigation routines.

$$
\begin{aligned}
& \text{Two-Way Geometric Range,} \\
2R\mid_{t_e} &= c(t_e - t_s) + (\Delta\rho_1 + \Delta\rho_2) = c(t_e - t_s) + \Delta\rho \\
& \text{Two-Way Pseudorange,} \\
\rho &= c\left[(t_e + \psi\mid_{te}) - (t_s + \psi\mid_{ts})\right] + \Delta\rho + c\Delta_{xx} + c\Delta_{xr} \\
& \quad +c(\psi|_{te} - \psi|_{ts}) + \nu \\
&= c(t_e - t_s) + \Delta\rho + c\delta t + c(\Delta_{tx} + \Delta_{xr}) + \nu \\
&= 2R\mid_{t_e} + c(\psi\mid_{te} - \psi\mid_{ts}) + c(\Delta_{tx} + \Delta_{xr}) + \nu \qquad (2.2)
\end{aligned}
$$

where

$R\mid_{t_e}$ = True scalar range at signal receipt (end)

t_s = System time at which the original signal left the transceiver

t_e = System time at which the return signal reached the transceiver

$\Delta\rho_1$ = Change in position of transceiver during time-of-flight projected along the line-of-sight direction

$\Delta\rho_2$ = Change in position of transponder during return trip projected along the line-of-sight direction

Δ_{xx} = Transceiver transmit line delay

Δ_{xr} = Transceiver receive line delay

$$
\begin{aligned}
\psi|_{ts} &= \psi(t_s) = \text{Clock state at } t_s \\
\psi|_{te} &= \psi(t_e) = \text{Clock state at } t_e \\
\delta t &= \psi\ |_{ts} + \psi\ |_{te} = \text{Overall clock bias contribution} \\
c &= \text{Speed of light} \\
\nu &= \text{Unmodelled error contributions}
\end{aligned}
$$

2.1.3 Sensor Architecture

The sensor hardware for one-way and two-way ranging share many attributes. Sample architectures are shown in Figures 2.5 and 2.6. As these figures show, the two-way method can be thought of as an extended case of the one-way method with each member having both transmit and receive capabilities. Measuring time-of-flight of a radio signal generally involves a phase measurement from either a generated code or the carrier wave itself. Both the signal generation and measurement processes utilize a local frequency standard, typically in the form of a thermally-controlled (TXCO) or numerically-controlled (NCO) oscillator. For increased ranging and navigation accuracy, one or both may have an ultra-stable oscillator (USO). All radionavigation systems have line biases associated with the transmission and receiver hardware as well.

A key consideration for the two-way measurement type is the time delay in retransmission of the signal at the transponder. As Figure 2.6 shows, there

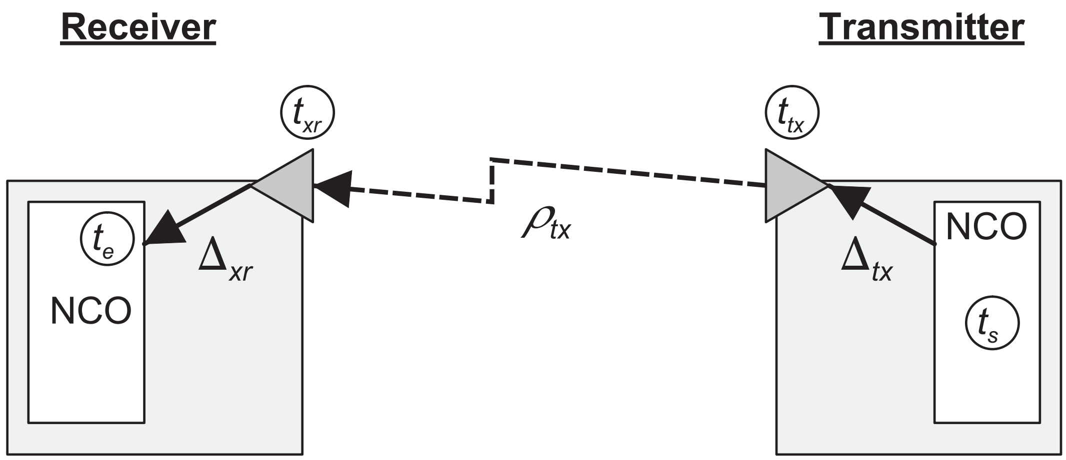

Figure 2.5: 1-Way RF Measurement Type

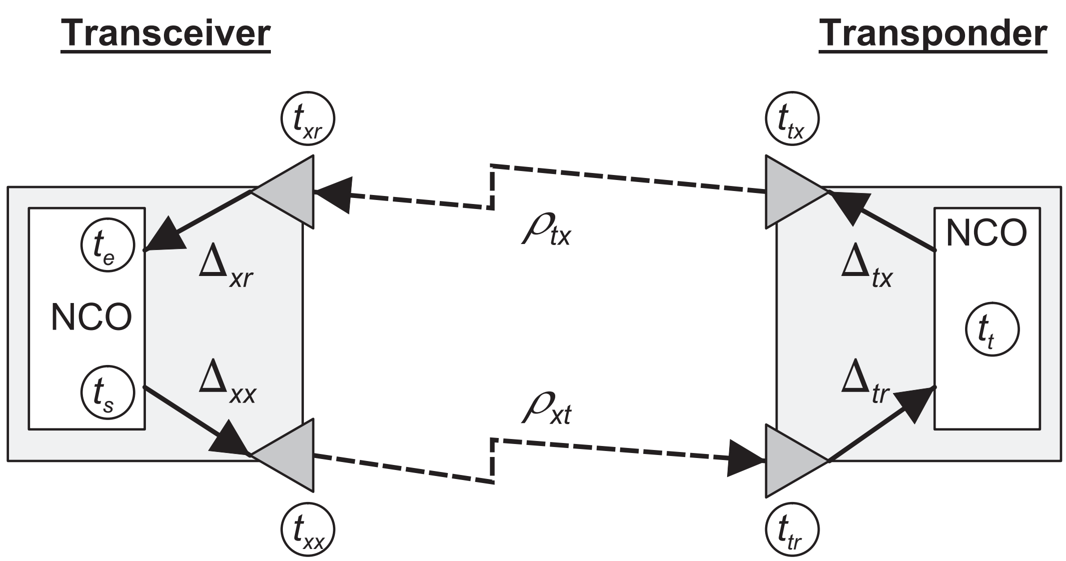

Figure 2.6: 2-Way RF Measurement Type

are line biases and internal effects that can contribute error to the pseudorange. A solution to this is proposed by Ely [17], where a phase-coherent turnaround scheme is used to essentially remove these biases and have the transponder function as a true signal reflector.

2.2 Clock Considerations

Any timed radionavigation solution will depend upon a reference oscillator, or clock, to generate signals for transmission and/or phase comparison. Any unmodelled errors in the clock will propagate through the solution process as errors in navigation. An offset of 1 msec can translate to a 300-km error in pseudorange[25]. Clock error modelling and removal, then, becomes an important part of the radionavigation solution. The clock bias is modelled as a random walk process associated with the integral of the white noise oscillator frequency [17]. To estimate the clock state in a navigation filter, this is typically represented by a Taylor series expansion as in Equation 2.3.

$$\phi(t) = \phi(t_0) + d_0(t - t_0) + a_0(t - t_0)^2 + \ldots \tag{2.3}$$

where

$$\begin{aligned} t_0 &= \text{Reference epoch for clock parameters} \\ \phi(t_0) &= \text{Clock bias } (sec) \\ d_0 &= \text{Clock drift } (sec/sec) \\ a_0 &= \text{Frequency drift } (sec/sec^2) \end{aligned}$$

The state vector for the satellite can include any number of these clock terms, but typically just the first two are considered. As will be shown later in the simulations, these two terms will give a good representation of the clock for the filter models used in the following chapters.

When constructing a navigation simulation, realistic clock performance is important since it is typically the dominant error source in the pseudorange measurement. A detailed explanation of clock models can be found in Parkinson [37], where the standard metric of *power spectral density* is defined for frequency stability. In simulations for this study, standard oscillators are modelled with white noise power spectral densities and of $4 \times 10^{-19}(m^2/sec)$ and $1.58 \times 10^{-18}(m^2/sec^3)$, while ultra-stable oscillators are modelled with $2 \times 10^{-26}(m^2/sec)$ and $7.89 \times 10^{-25}(m^2/sec^3)$ [27].

Chapter 3

Low Earth Orbit

The Low Earth Orbit (LEO) environment, generally defined as below 5,000 km altitude, contains the vast majority of existing and future satellite missions [46]. Formation flying navigation in this region greatly benefits from the presence of GPS. Because of the measurement rich environment, passive one-way ranging sensors (GPS receivers) are particularly effective for relative navigation. As was encountered in the development of the FASTRAC mission, attitude determination using GPS can be challenging. When using a single uniform-gain antenna, the solution is indeterminate about the antenna boresight direction. This motivated the development of a method to obtain more measurement information. If an additional sensor, such as a magnetometer, could be incorporated then the estimate would be improved.

3.1 Filtered Sensor Combinations

A spacecraft navigation or attitude filter is generally only as accurate as the measurements with which it is provided. Measurements from a single source, however, can prove inaccurate in certain operating regimes. By adding additional sensors and measurements, the filter can improve its overall accuracy and, more importantly, operate in regions where single measurements would make the problem unobservable.

3.1.1 GPS SNR and Magnetometer

The motivation of this problem was to resolve the yaw ambiguity in a GPS single antenna attitude estimate. As a GPS receiver tracks the signal from a GPS satellite, it will compute the signal-to-noise ratio (SNR). This ratio is primarily affected by the gain pattern of the antenna used by the receiver. Utilizing GPS SNR and magnetometer measurements is a method of obtaining coarse attitude determination for a spacecraft. The GPS SNR measurement type is shown in Figure 3.1. There are three vectors that contribute to the solution: the antenna boresight vector, $\vec{A}$, the GPS line-of-sight vector, $\vec{L}$, and the local magnetic field vector, $\vec{b}_m$. The measured SNR is mapped to a modelled antenna gain pattern to form this measurement type, shown in Equation 3.1. This method was first explored by Axelrad and Behre to generate single pointing vector solutions [4]. Dunn and Duncan used a similar technique to obtain point vector solutions that were accurate to within 15 degrees on the Microlab-1 satellite [15]. Full three-axis attitude solutions were computed by Buist, et al [9] using a single antenna on a gravity gradient stabilized satellite known as PoSAT-1. In this case, the presence of a gravity gradient boom created variation in the azimuthal gain pattern of the antenna which was combined with the gravity gradient dynamics to generate solutions that agreed to within 10 degrees of those derived independently using a magnetometer.

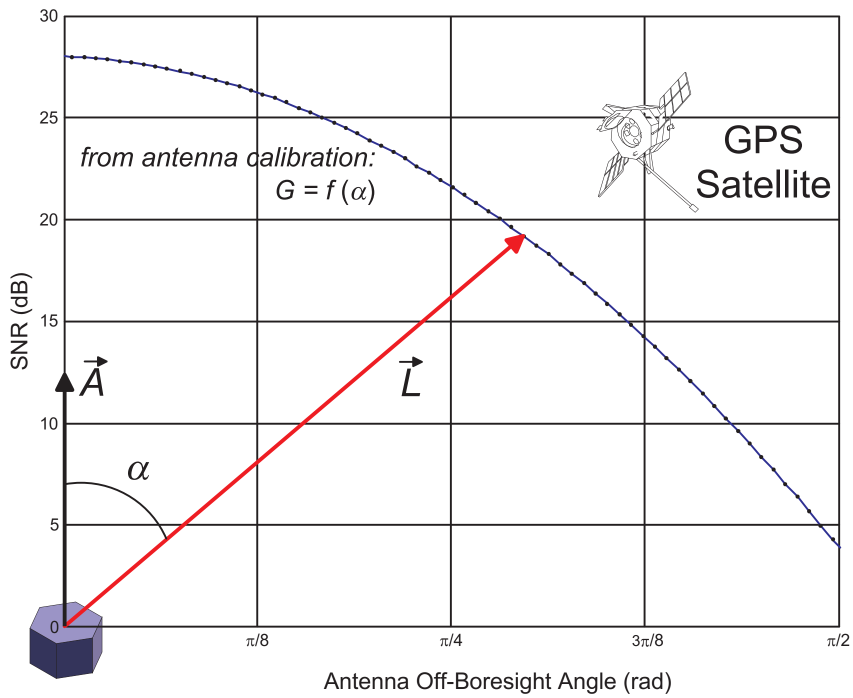

Figure 3.1: GPS SNR Off-Boresight Vector

For a complete derivation of the filter setup, see Stewart [40]. To summarize, the magnetometer measurement is taken as a quaternion rotation about the spacecraft boresight, as shown in Equation 3.2. These measurement types are incorporated into the Extended Kalman Filter as shown in Equation 3.3.

$$
\begin{aligned}
G_{GPS} &= \mid \vec{A} \cdot \vec{L} \mid = f(\alpha) = c_0 + c_1\alpha + c_2\alpha^2 && (3.1)\\
G_{MAG} &= \bar{b}_{rot} = (2q_0^2 - 1)\bar{b}_m + 2(\bar{q} \cdot \bar{b}_m)\bar{q} + 2q_0(\bar{q} \times \bar{b}_m) && (3.2)\\
H &= \frac{\partial G}{\partial X} = \begin{bmatrix} \widetilde{H}_{GPS1} \\ \vdots \\ \widetilde{H}_{GPSn} \\ \widetilde{H}_{MAG1} \\ \vdots \\ \widetilde{H}_{MAG3} \end{bmatrix}_{[(ngps+3)\times 3]} && (3.3)
\end{aligned}
$$

Unique $\widetilde{H}$ vectors are required for the GPS signal-to-noise ratio measurements as well as each component of the magnetometer measurement. Essentially, each reported component of the measured magnetic field vector is treated as an individual scalar measurement, and processed accordingly. These equations are greatly simplified by aligning the GPS antenna boresight direction with the body z-axis:

$$
\widetilde{H}_{GPS}^T = -2 \begin{bmatrix} -x_3 & x_2 & 2x_1 \\ x_4 & x_1 & 0 \\ -x_1 & x_4 & 0 \\ x_2 & x_3 & 2x_4 \\ 0 & 0 & 0 \\ 0 & 0 & 0 \\ 0 & 0 & 0 \end{bmatrix} \cdot \begin{bmatrix} L_x \\ L_y \\ L_z \end{bmatrix} \tag{3.4}
$$

$$\widetilde{H}^T_{Mag1} = 2\begin{bmatrix} 2x_1b_{m1} + x_3b_{m3} - x_4b_{m2} \\ 2x_2b_{m1} + x_3b_{m2} + x_4b_{m3} \\ x_2b_{m2} + x_1b_{m3} \\ x_2b_{m3} - x_1b_{m2} \\ 0 \\ 0 \\ 0 \end{bmatrix} \tag{3.5}$$

$$\widetilde{H}^T_{Mag2} = 2\begin{bmatrix} 2x_1b_{m2} + x_4b_{m1} - x_2b_{m3} \\ x_3b_{m1} - x_1b_{m3} \\ 2x_3b_{m2} + x_2b_{m1} + x_4b_{m3} \\ x_3b_{m3} + x_1b_{m1} \\ 0 \\ 0 \\ 0 \end{bmatrix} \tag{3.6}$$

$$\widetilde{H}^T_{Mag3} = 2\begin{bmatrix} 2x_1b_{m3} + x_2b_{m2} - x_3b_{m1} \\ x_4b_{m1} + x_1b_{m2} \\ x_4b_{m2} - x_1b_{m1} \\ 2x_4b_{m3} + x_2b_{m1} + x_3b_{m2} \\ 0 \\ 0 \\ 0 \end{bmatrix} \tag{3.7}$$

3.2 Matlab Simulation

Building on work from Madsen[30] and Stewart[40], a Matlab simulation was written that post-processes logged GPS data to produce an attitude solution. The SNR values are logged at 1 Hz and later read in as bulk data to be processed in the filter. Inside the simulation, a magnetometer is modelled and used in the attitude filter. The true attitude state is also logged by the GPS simulator and a comparison with the estimate is made.

3.3 Embedded Hardware

Many modifications were needed to convert the theoretical attitude determination algorithm originally coded in Matlab into a workable, embedded flight system for use on an actual satellite.

3.3.1 Memory and Channel Allocation

First, the original MATLAB was ported into C and embedded into the existing GPS receiver source code. There were numerous issues with memory allocation and array sizing to make the code stable on the ARM60 microcontroller, but these were resolved by clearing stack space before the covariance update in the Extended Kalman Filter routine. The code runs with approximately 20% margin in processing capability. An additional problem was encountered in the allocation of receiver channels to a specific tracked GPS satellite vehicle. As satellites drop out of view of the receiver, a new satellite is allocated to the channel. The code accumulator initializes the bit-synchronization process on the new satellite and begins to receive the 50 Hz GPS navigation message. As soon as the message is received, the receiver will lock onto the navigation subframe and begin pseudorange measurements. The master satellite index, however, does not update until the navigation message is fully processed which can result in erroneous measurements for around 5 seconds. To account for this, the attitude algorithm looks for large pseudorange changes on a channel where there has not been a satellite reallocation and damps this change until the new satellite index appears. The damping occurs by scaling with a small, nonzero constant to avoid matrix singularities.

3.3.2 Receiver Interface

There was also an implementation of an interface for receiving and processing external magnetometer inputs. The magnetometer measurement is necessary to avoid the observability problem brought on by the assumption of an azimuthally symmetric antenna gain pattern. Without this measurement, the rotation about the antenna boresight vector would be indeterminant. An external interface was developed to provide the algorithm with once per second measurement updates from the spacecraft magnetometer.

3.3.3 Filter Equations

In Stewart [40], the measurement equations were all derived in a North-East-Down frame typically used for aircraft attitude determination. Figure 3.2, however, shows an orbital reference frame, such as the Radial-Along Track-Cross Track (RSW) frame, more often used for spacecraft analysis. The filter equations for the flight hardware are reworked for the RSW frame instead of NED, which is much more useful in an orbital environment for avoiding large reference frame motion and for supplying attitude inputs to a spacecraft control system. For example, in a high inclination orbit the East direction will trend toward a singularity near the poles. The GPS native measurement coordinate system is Earth-Centered, Earth-Fixed using the WGS-84 reference ellipsoid, so the line-of-sight position measurements were converted to RSW

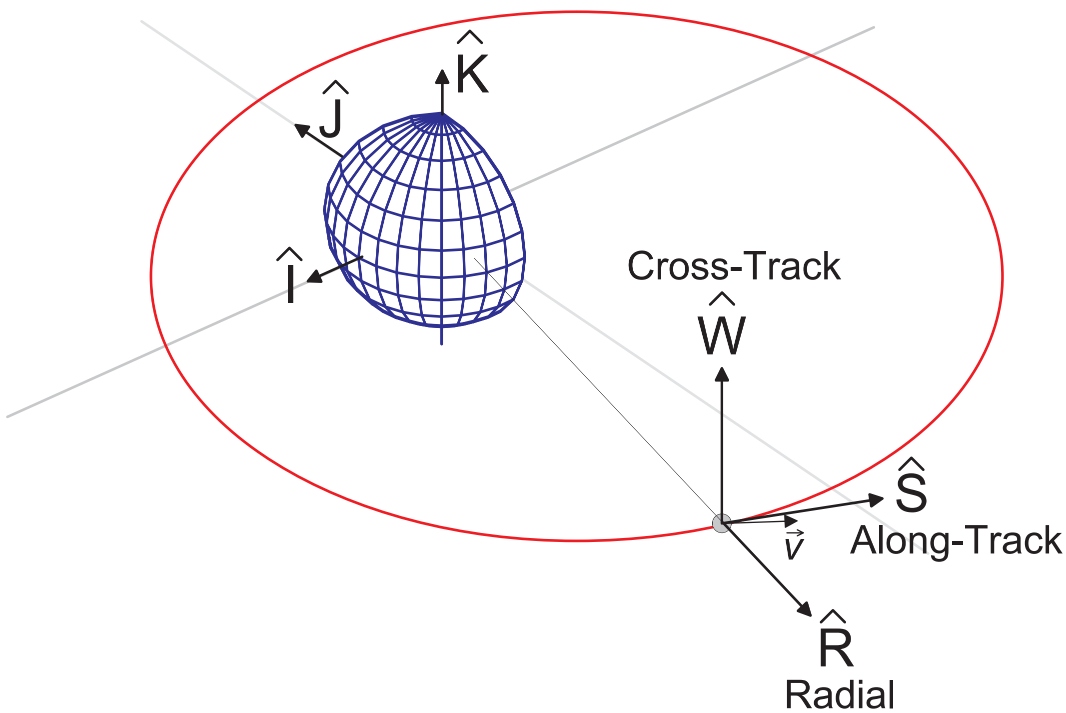

Figure 3.2: Orbital Reference Frame, RSW

before processing using the transformation in Equation 3.8.

$$\vec{V}_{RSW} = \left[\widetilde{R}|\widetilde{S}|\widetilde{W}\right]\vec{V}_{ECEF} \tag{3.8}$$

where

$$\begin{aligned}
\widetilde{R} &= \vec{R}_{ECEF}/||\vec{R}_{ECEF}|| \\
\widetilde{W} &= \vec{R}_{ECEF} \times \vec{V}_{ECEF} \\
\widetilde{S} &= \vec{R}_{ECEF} \times \widetilde{W}
\end{aligned}$$

3.4 Hardware Testing

Extensive testing was performed to validate the attitude determination algorithms and evaluate the expected performance of this formation flying sensor in its expected operational environment. This section details the setup and results of that effort.

3.4.1 Constellation Simulator

A hardware testbed was developed to evaluate the embedded software. Two engineering model GPS units with the embedded attitude determination code were used as the primary sensors. Each unit was connected to a single GPS RF constellation simulator (SPIRENT) and data collection PC. The constellation simulator is capable of replicating with high fidelity the RF environment experienced in Low Earth Orbit. Simulated, synchronized magnetometer measurements were also supplied to the GPS units at 1 Hz. The

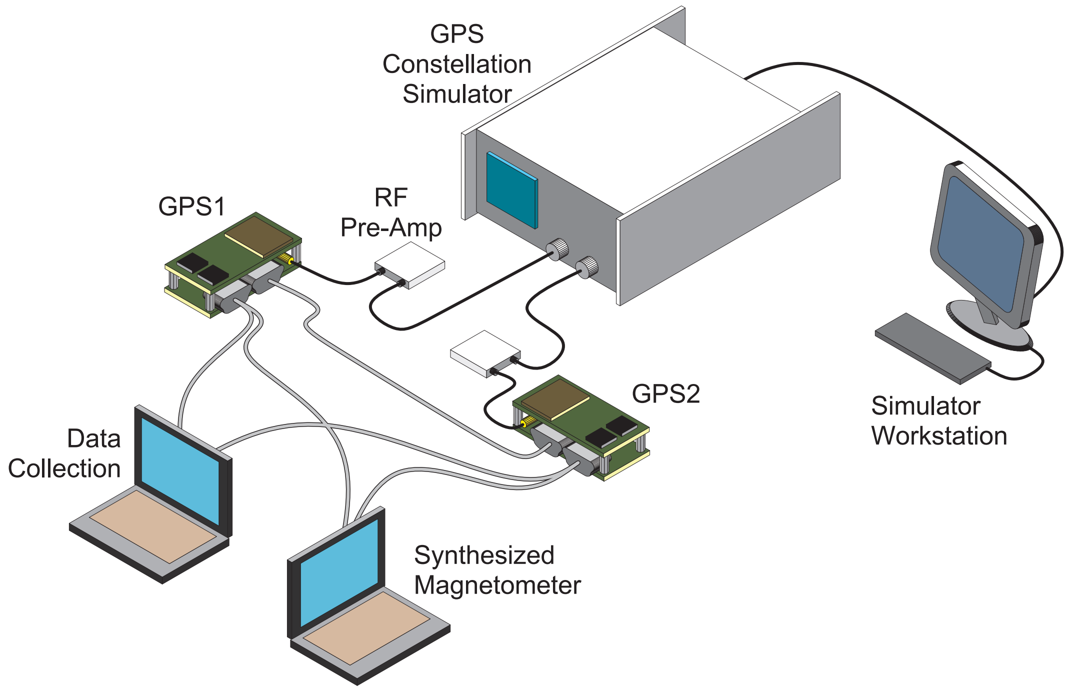

Figure 3.3: GPS Hardware/Simulator Setup

setup is shown in Figure 3.3. This setup allows the sensor to perform all its on-board navigation functions simultaneously: absolute navigation, relative navigation, and attitude determination.

3.4.2 Synthesized Magnetometer Measurements

In the actual spacecraft, a magnetometer is sampled by the flight computer and the data is relayed to the GPS units for use in their EKF routines. For the hardware testbed, some other measurement must be provided since the actual magnetometer would not return the correct magnetic field values while physically located in the laboratory. By using the repeatability of the constellation simulator, these values can be simulated in real-time and provided to the GPS receiver just as they would from the spacecraft flight computer.

Because the constellation simulator logs the true vehicle state, knowledge of the vehicle position and attitude is available at any time during the run. Using the information logged from a previous run, a separate PC operating Matlab calculates the IGRF2000 magnetic field model in real-time and rotates that vector into the body-fixed spacecraft frame. Oncer per second this data is formatted according to the flight computer specifications and sent to the GPS where it is stored for use during the next filter iteration. The magnetometer simulation PC is initialized at the same time as the simulator to synchronize the data.

3.4.3 Results

An identical simulation was performed with the embedded GPS code and the MATLAB code to compare the ported software with the originally designed algorithm. It consisted of a slow yaw from 0 to 30 degrees, while pitch and roll were held constant at zero. The spacecraft rate was a maximum of 0.001 rad/sec. Figure 3.4 shows the Matlab and embedded quaternion elements compared to the true simulated attitude. Figure 3.5 shows this same data converted to a standard aircraft Euler sequence of Roll-Pitch-Yaw for more convenient visualization. The estimated solution agrees to within 10 degrees of the true attitude for this scenario. This is considered to be a reasonable level of accuracy for this algorithm. Though within expected accuracy, there are some disagreements between the MATLAB and embedded hardware. Some of this may be explained by the once-per-second magnetometer updates to the embedded hardware. Under worst case output times, the measurements may be up to one second old when processed.

3.5 Software Simulation

A software simulation was written to further examine the LEO measurement environment and to evaluate the sensor models described in the previous chapter. A snapshot of the simulation environment is shown in Figure 3.6. The orbit is nominally 1000 km altitude and 45^o inclination. The GPS satellite orbits are derived and propagated from the published ephemeris set for GPS week 1210.

3.5.1 Dilution of Precision

All line-of-sight based ranging systems have geometrical observability considerations that affect navigation accuracy. This geometry can be quantified by a dimensionless scale factor known as the Dilution of Precision (DOP).

$$Acc = DOP \times \sigma_{UERE} \tag{3.9}$$

where

$$\begin{aligned} Acc &= \text{Positioning Accuracy } (m) \\ \sigma_{UERE} &= \text{User Equivalent Range Error } (m) \end{aligned}$$

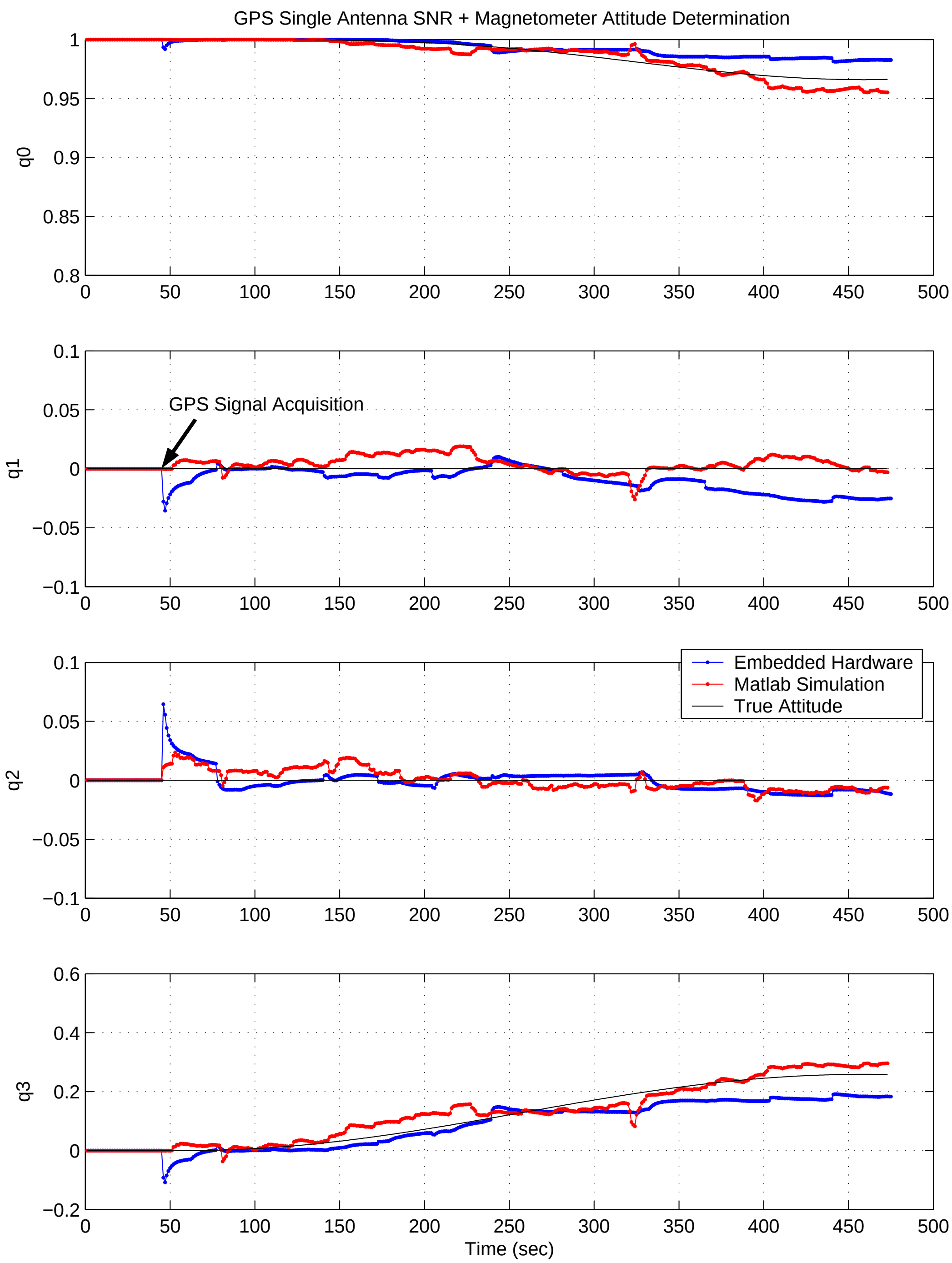

Figure 3.4: Post-Processed Matlab Results, Quaternions

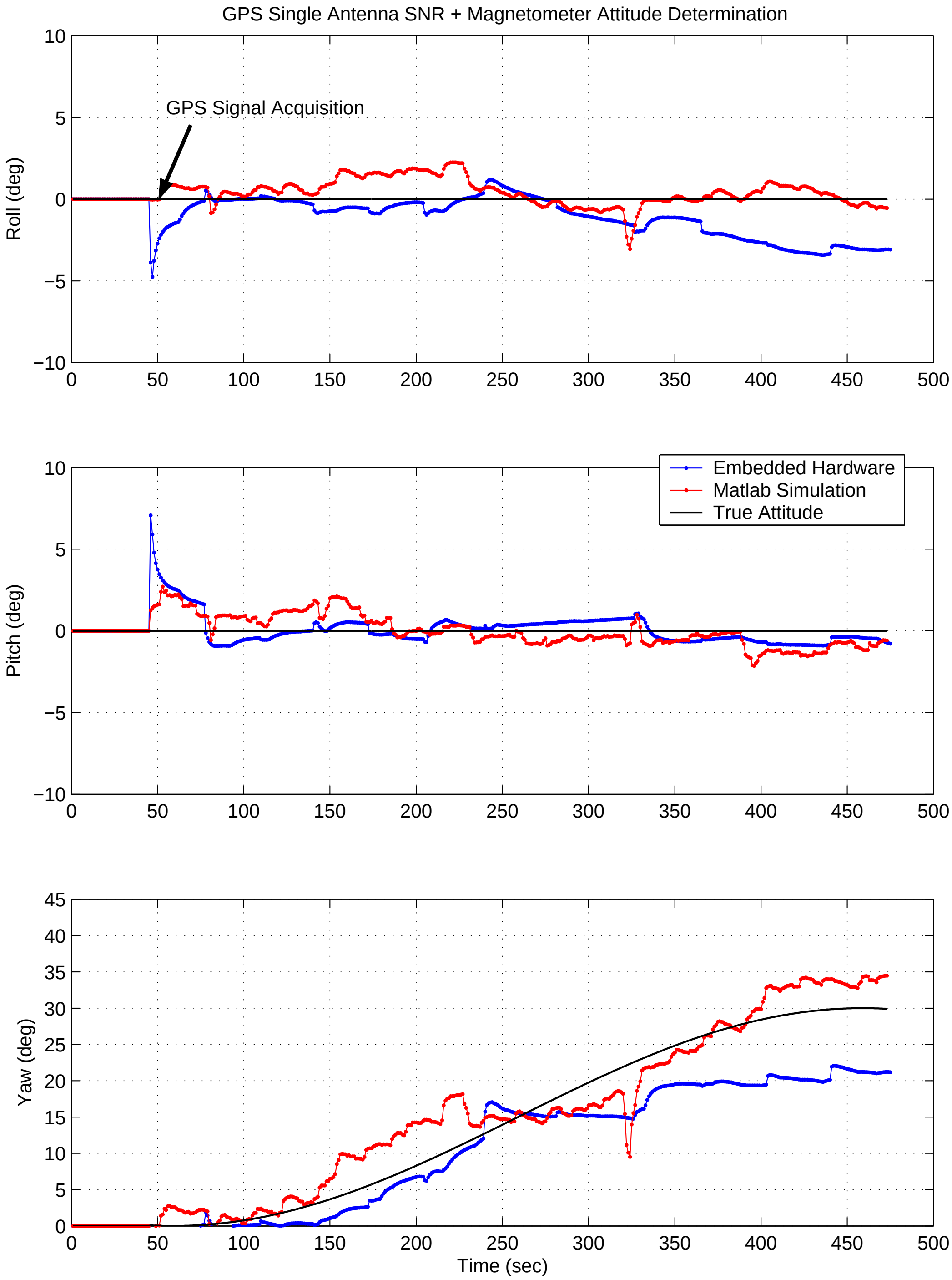

Figure 3.5: Post-Processed Matlab Results, Euler Angle Error

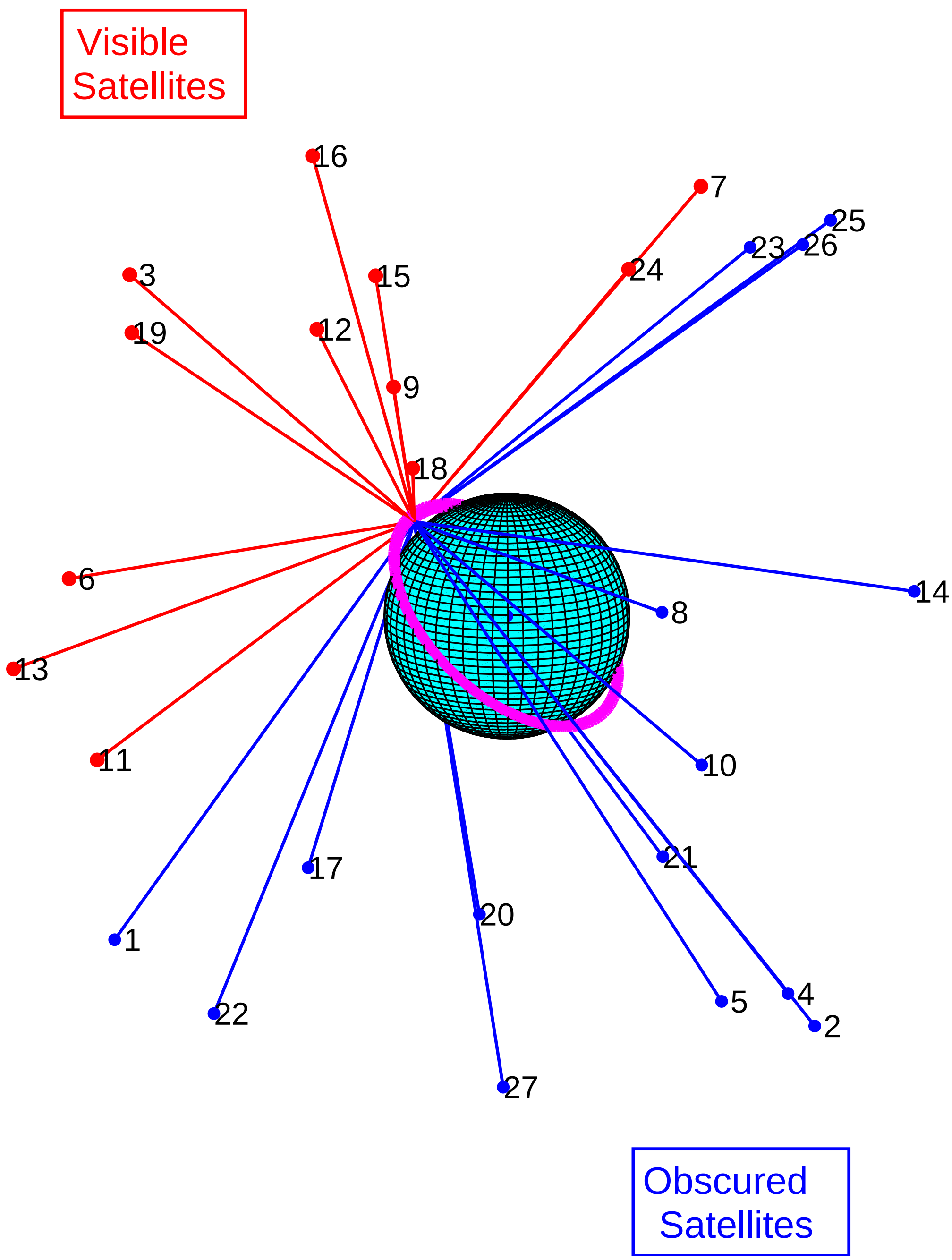

Figure 3.6: Simulated LEO Geometry Snapshot

The σ_{UERE} is the sum of the contributions from each of the error sources associated with a particular GPS satellite. It is typically approximated by a zero mean Gaussian random variable. The cofactor matrix used by the positioning algorithm can be analyzed for DOP as a measure of the geometric distribution of satellites relative to the receiver. Each diagonal element of the cofactor matrix corresponds to the square of the DOP value along a particular axis, as shown in Equation 3.10.

$$\left(H^T H\right)^{-1} = \left[\begin{pmatrix} XDOP^2 & - & - & - \\ - & YDOP^2 & - & - \\ - & - & ZDOP^2 & - \\ - & - & - & TDOP^2 \end{pmatrix}\right] \tag{3.10}$$

The overall geometric distribution can be quantified by the single quantity Geometric Dilution of Precision (GDOP). It is defined as

$$GDOP = \sqrt{XDOP^2 + YDOP^2 + ZDOP^2 + TDOP^2} \tag{3.11}$$

A more detailed explanation can be found in Hofmann[23].

3.5.2 LEO Results

Figure 3.7 shows the error components of a simulated GPS receiver in a LEO environment. The results are presented in an RSW frame, and as expected the radial component shows the highest root-sum-square (RSS) error result. The DOP can be rotated into any reference frame, and in this case has been rotated into the RSW frame to coincide with the error residuals. Figure 3.8 shows the combined error in all axes and its correlation with the (GDOP), which is the combined DOP in all axes. Figure 3.9 shows the clock estimator performance, along with the Time Dilution of Precision (TDOP). Although TDOP does not coincide with any specific geometric axis, it does provide a measure of the ability of the estimation filter to accurately model the clock at any given epoch.

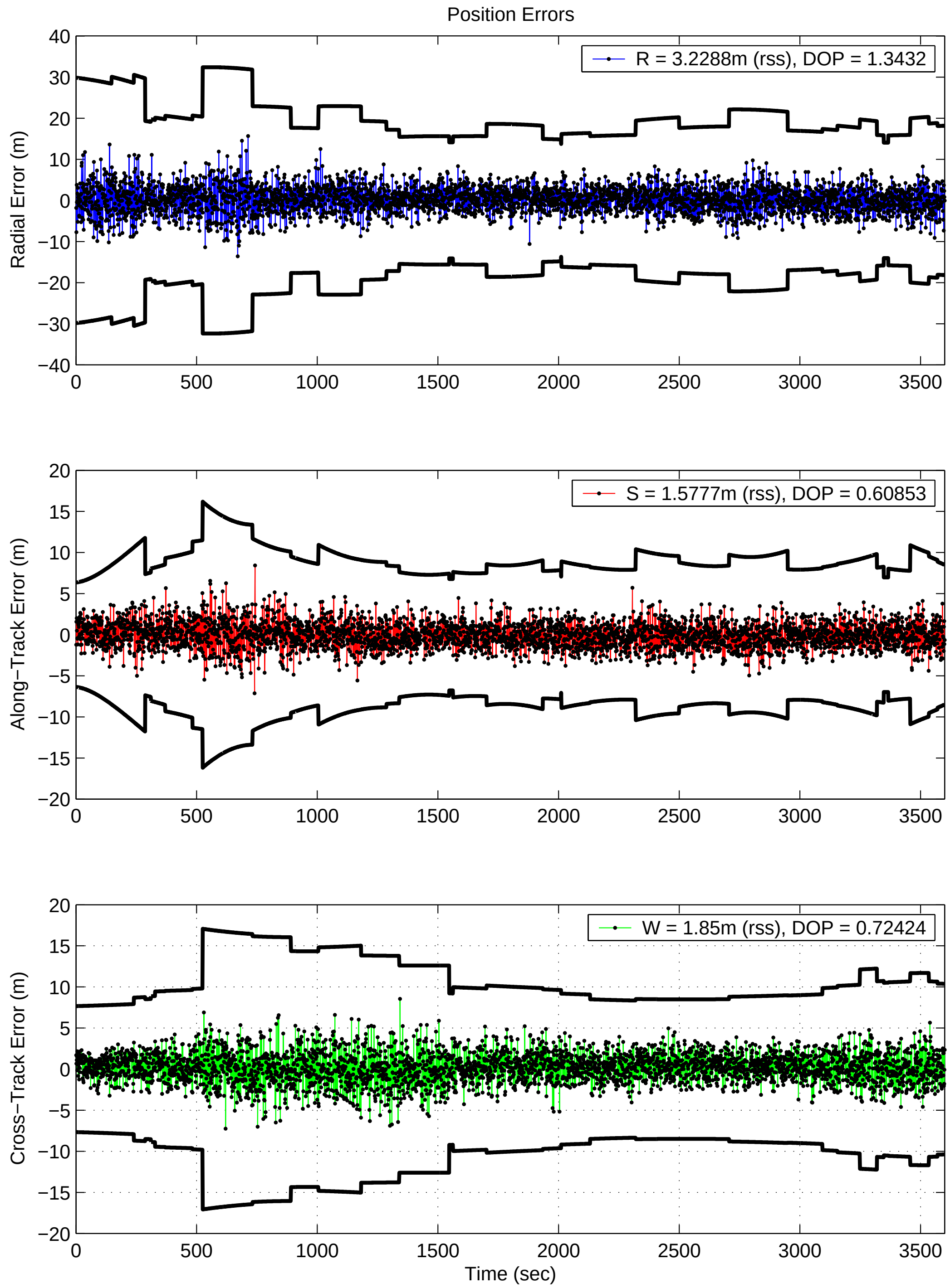

Figure 3.7: LEO GPS Estimated Position Error Components

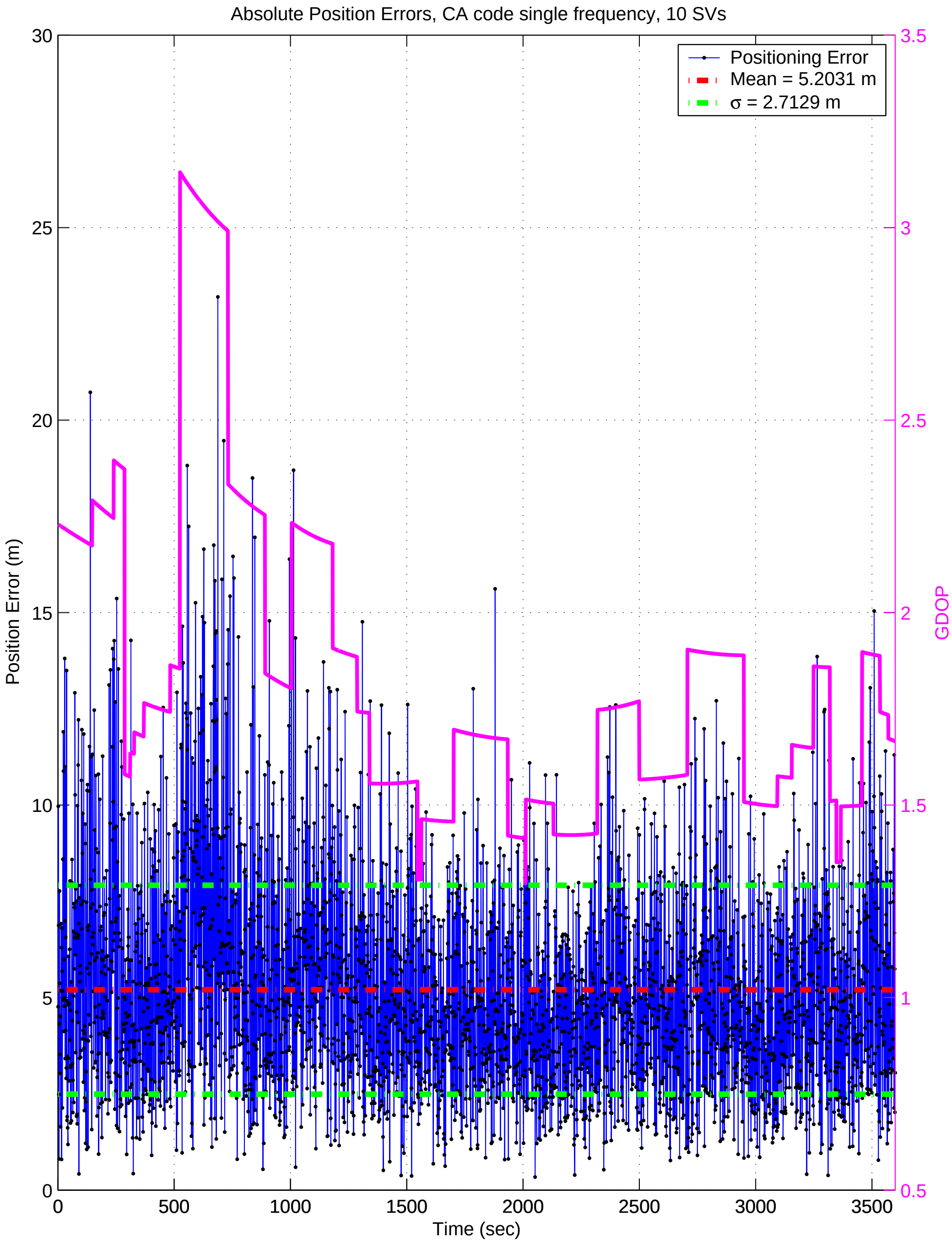

Figure 3.8: LEO GPS Estimated Position Error Shown With GDOP

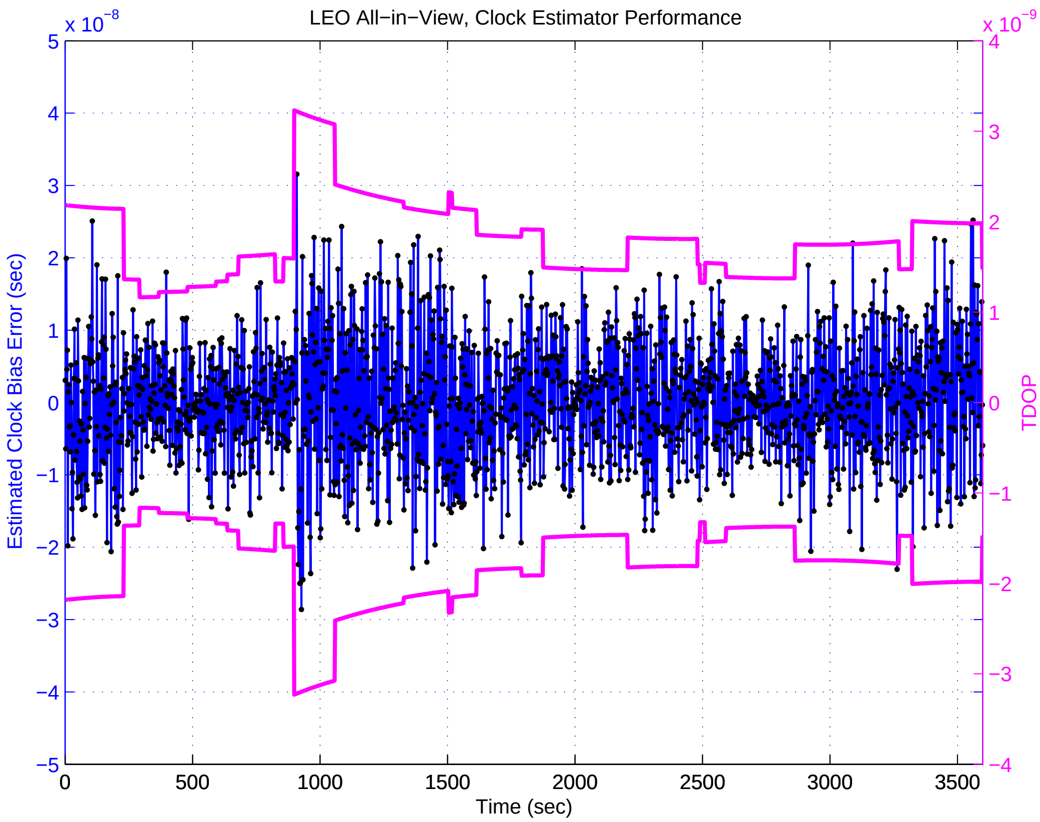

Figure 3.9: LEO GPS Estimated Clock Bias Errors

Chapter 4

Highly Elliptical Orbit

A satellite formation in a highly elliptical Earth orbit (HEO) is of great interest to many mission designers. Carpenter, et. al. describe a HEO formation, the Magnetospheric Multi-Sclae Mission (MMS), as a benchmark problem [11]. The navigation task, however, becomes increasingly difficult as the distance from Earth increases. Specifically, the signals from the terrestrial Global Positioning System satellites become harder to track and in many cases are altogether unavailable. It may be necessary, therefore, to augment the formation navigation capability using additional sensors to achieve needed navigation performance. RF transceiver measurements between formation members have been proposed as one method of supplying this additional information.

4.1 HEO Challenges

There are several difficulties with formation navigation in HEO. First, the relative equations of motion are different than in the simplified, circular LEO case. The nature of the orbit also dictates that there may be substantial amounts of time when the formation must navigate without the use of GPS. An estimation technique must be devised which takes into account the different types of measurements that will be used.

This type of formation, depending upon mission requirements, may require the use of a combination of sensors. Utilizing the GPS constellation when near the Earth allows the navigation filters to fine-tune the vehicle state estimates at least once per orbit. When the satellite is outside the GPS constellation, alternative sensors provide needed measurement updates.

4.2 HEO Simulation

The formation that was simulated for this study was based upon the benchmark orbit suggested by Carpenter [11]. This study was performed as an example of many typical applications. Although the details vary from case to case, the estimation process is general. For this study, the sensor models developed in the previous chapters were implemented into a MATLAB simulation of elliptical orbit dynamics. The reference orbit is summarized in Table 4.1 and shown in Figure 4.1.

The reference trajectory is propagated under the influence of Earth's gravity and some of the major perturbing forces of the terrestrial orbital environment. The perturbations include:

1. *Non-Spherical Gravity*

   The effect of asymmetric Earth gravity is modelled by inclusion of the

Table 4.1: Simulated HEO Orbit Mean Elements

Element	Value	Units
a	61277	km
e	0.875	none
i	0	deg
Ω	0	deg
ω	90	deg

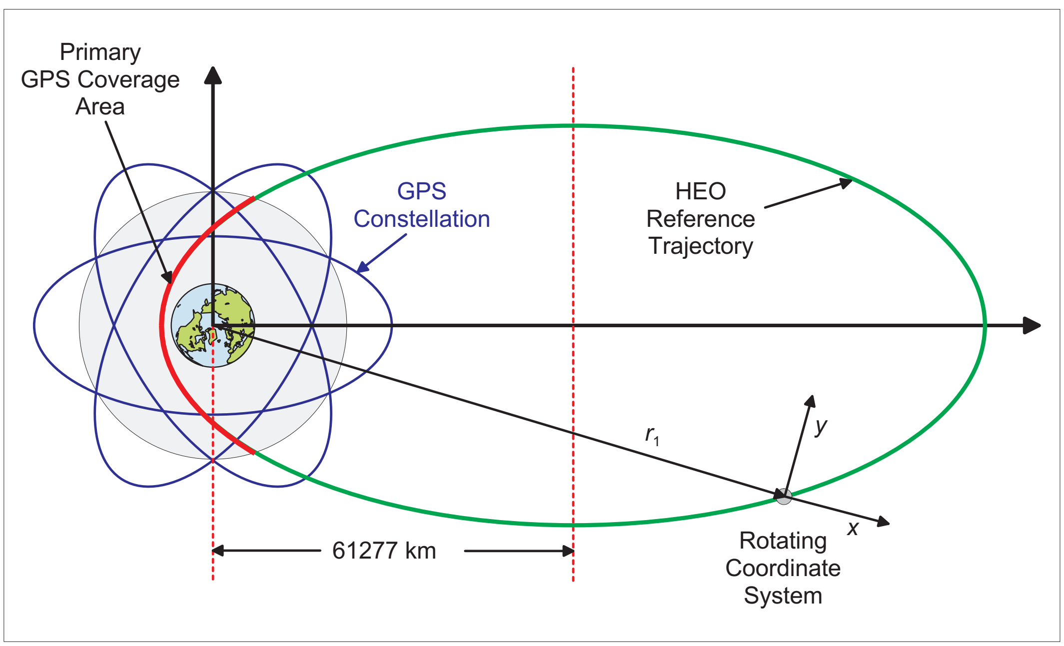

Figure 4.1: HEO Reference Trajectory, baselined in Carpenter[11]

effect of the first spherical harmonic term, commonly known as J2 [45].

$$\begin{aligned} a_i &= \frac{-3J_2\mu R_\oplus^2 r_i}{2r^5}\left(1-\frac{5r_k^2}{r^2}\right) \\ a_j &= \frac{-3J_2\mu R_\oplus^2 r_j}{2r^5}\left(1-\frac{5r_k^2}{r^2}\right) \\ a_k &= \frac{-3J_2\mu R_\oplus^2 r_k}{2r^5}\left(3-\frac{5r_k^2}{r^2}\right) \end{aligned} \tag{4.1}$$

where

$$\begin{aligned} \vec{a} &= a_i\hat{i} + a_j\hat{j} + a_k\hat{k} = \text{acceleration } (m/s^2) \\ \mu &= \text{Earth gravitational parameter } (m^3/s^2) \\ R_\oplus &= \text{Earth radius } (m) \\ r_{i,j,k} &= \text{Satellite position vector components in Earth Centered frame } (m) \\ r &= \text{Radius of satellite orbit } (m) \end{aligned}$$

2. *Lunar Third Body Effects*

The gravitational interaction of the moon with both the satellite and the Earth were modelled [45].

$$\vec{a} = -\frac{\mu_\oplus \vec{r}_{\oplus-sat}}{r_{\oplus-sat}^3} + \mu_M\left(\frac{\vec{r}_{sat-M}}{r_{sat-M}^3} - \frac{\vec{r}_{\oplus-M}}{r_{\oplus-M}^3}\right) \tag{4.2}$$

where

$$\begin{aligned} \mu_\oplus &= \text{Earth gravitational parameter} \\ \mu_M &= \text{Moon gravitational parameter} \\ \vec{r}_{\oplus-sat} &= \text{Vector from Earth to Satellite} \\ \vec{r}_{sat-M} &= \text{Vector from Satellite to Moon} \\ \vec{r}_{\oplus-M} &= \text{Vector from Earth to Moon} \end{aligned}$$

3. *Atmospheric Drag*

As the formation nears Earth at perigee, it is subject to drag in the upper levels of the atmosphere. This drag was modelled with assumed values for mass and drag coefficient [45]. The relative velocity between satellite and atmosphere was calculated with an assumed stationary atmosphere.

$$\vec{a} = -\frac{1}{2}\rho\frac{C_D A}{m}|v|\overrightarrow{v}; \tag{4.3}$$

where

$$\begin{aligned} \rho &= \text{Atmospheric density } (kg/m^3) \\ \frac{m}{C_D A} &= \text{Satellite ballistic coefficient } (kg/m^2) \\ \vec{v} &= \text{Relative velocity between satellite and atmosphere } (m/s) \end{aligned}$$

4.2.1 Formation Setup

The simulated formation is built around the reference trajectory previously described, however there is no spacecraft on the reference trajectory. The four spacecraft which make up the formation must form a 10 km regular tetrahedron at apogee. Close approaches of 1 km or less are prohibited in the specification.

This orbit is accomplished using the initial offsets from the nominal reference trajectory shown in Table 4.2.

The formation relative motion is shown in Figure 4.2. The motion is shown relative to the HEO reference trajectory in Figure 4.1. At apogee,

Table 4.2: Initial Formation Offsets

Offset	Sat 1	Sat 2	Sat 3	Sat 4
x_{rel} (m)	0	5000	-5000	0
y_{rel} (m)	$10000/\sqrt{3}$	$-5000/\sqrt{3}$	$-5000/\sqrt{3}$	0
z_{rel} (m)	0	0	0	$10000\sqrt{2/3}$
$\dot{x}_{rel}$ (m/s)	0	0.05	0.05	0
$\dot{y}_{rel}$ (m/s)	0	-0.258	0.258	0
$\dot{z}_{rel}$ (m/s)	0	0	0	0

the formation assumes the regular tetrahedron specified in the requirements. Near perigee, however, the formation tends to "flatten" and actually becomes planar in two places. The formation separation distances are shown in Figure 4.3. There are no approaches within the specified 1 km exclusion area.

4.3 Estimation Technique

For simulations in this study, an eight element relative state vector was used consisting of position, velocity, and local oscillator terms. The position and velocity components are all given relative to the reference orbit.

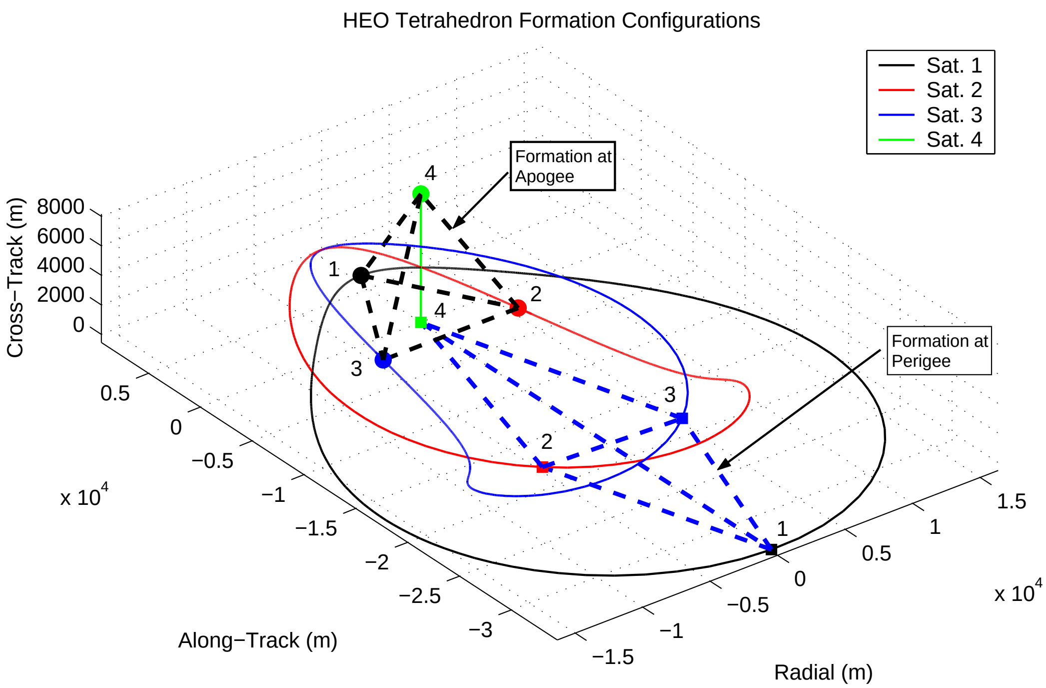

Figure 4.2: Tetrahedron Formation in HEO

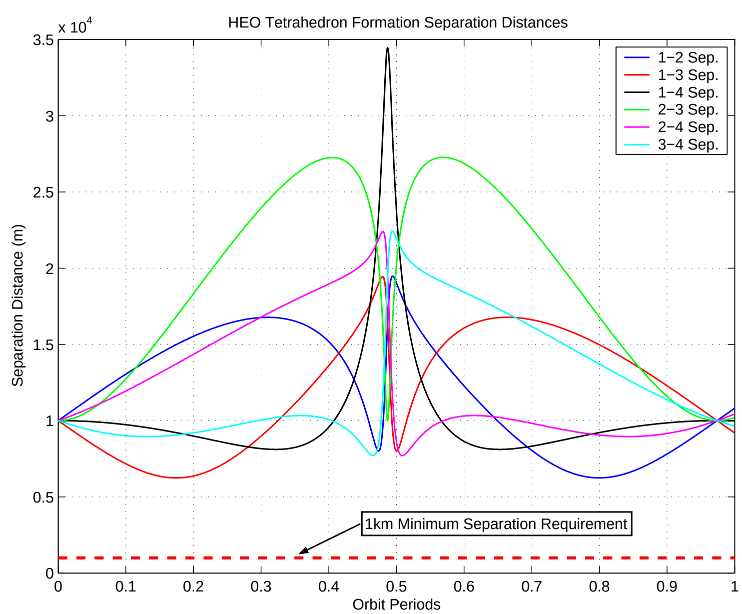

Figure 4.3: Tetrahedron Formation Separation Distances

$$\vec{X} = \begin{bmatrix} x_{rel} & (m) \\ y_{rel} & (m) \\ z_{rel} & (m) \\ \dot{x}_{rel} & (m/s) \\ \dot{y}_{rel} & (m/s) \\ \dot{z}_{rel} & (m/s) \\ c\delta t & (m) \\ c\delta\dot{t} & (m/s) \end{bmatrix}, \ c = \text{Speed of light } (m/s) \tag{4.4}$$

Estimating the relative states of satellites in the formation is accomplished by use of a Kalman Filter, also known as a sequential filter. The Kalman Filter is able to accumulate measurements over extended time intervals to improve its estimation accuracy. The type and weighting of measurements in the Kalman Filter will depend upon the particular orbit and sensors involved. The general form of the Kalman Filter is as follows[42]:

$$\text{Spacecraft State, } X\text{, from Eq. 4.4}$$

$$\text{Observation} = Y_i \ @ \ t_i$$

Propagate

$$\begin{aligned} \dot{X} &= F(X(t), t) \text{ from } X(t_{i-1}) \\ A(t) &= \frac{\partial F(X,t)}{\partial X} \\ \dot{\Phi}(t, t_0) &= A(t)\Phi(t, t_0) \text{ from } \Phi(t_{i-1}, t_{i-1}) = I \\ \overline{P}_i &= \Phi(t_i, t_{i-1})P_{i-1}\Phi^T(t_i, t_{i-1}) = \text{ Error Covariance Matrix} \end{aligned} \tag{4.5}$$

Accumulate Observations

$$
\begin{aligned}
y_i &= Y_i - G(X_i, t_i) \\
\widetilde{H}_i &= \frac{\partial G(X,t)}{\partial X} = \text{ Measurement Matrix} \\
K_i &= \overline{P}_i \widetilde{H}_i^T \left(\widetilde{H}_i \overline{P}_i \widetilde{H} i^T + R_i \right)^{-1} = \text{ Filter gain}
\end{aligned}
\tag{4.6}
$$

Update

$$
X_{i+1} = X_i + K_i y_i \tag{4.7}
$$

$$
P_{i+1} = (I - K_i H_i)\, \overline{P}_i + Q_i, \;\; Q_i = \text{ Process Noise Covariance}
$$

The Kalman filter dynamic model was derived from the relative equations of motion for bodies in elliptical orbits set out by Broucke [8]. These equations require knowledge of the reference orbit eccentricity (e), semi-major axis(a), and true anomaly(ν). The motion is assumed to be two-body, point mass dynamics with no perturbations based on the reference frame shown in Figure 4.1.

$$
\begin{aligned}
\ddot{x} - 2\dot{\theta}\dot{y} - \dot{\theta}^2 x - \ddot{\theta} y &= 2x \left(\frac{\mu}{r_1^3} \right) \\
\ddot{y} + 2\dot{\theta}\dot{x} - \dot{\theta}^2 y + \ddot{\theta} x &= -y \left(\frac{\mu}{r_1^3} \right) \\
\ddot{z} &= -\left(\frac{\mu}{r_1^3} \right)
\end{aligned}
\tag{4.8}
$$

where

$$
\begin{aligned}
r_1 &= \frac{a(1-e^2)}{(1+e\cos\nu)} \\
\dot{\theta} &= \sqrt{\mu(a(1-e^2))}/r_1^2 \\
\ddot{\theta} &= -2\mu e \sin\nu / r_1^3
\end{aligned}
$$

4.3.1 GPS-Only Estimation

One possibility for relative navigation of the formation is the use of GPS receivers and a simple data exchange crosslink. This allows absolute positioning and relative GPS.

4.3.1.1 GPS Visibility

To calculate visibility of individual GPS satellites in the simulation, two regimes were considered.

1. *Low Altitude* ($< \frac{3}{4}$ GPS Altitude)

Given an elevation mask α, compute the angle to an individual GPS satellite by

$$\theta = \cos^{-1}\left(\widehat{R} \cdot \overrightarrow{r}_{\mathrm{LOS}}\right) \tag{4.9}$$

where $\widehat{R}$ is the unit vector from Earth to the receiver and $\overrightarrow{r}_{\mathrm{LOS}}$ is the Line-of-Sight vector from the receiver to the GPS satellite under consideration. The

GPS satellite is then visible when

$$\theta_{\text{visible}} < 90^o - \alpha \tag{4.10}$$

2. *High Altitude* ($> \frac{3}{4}$ GPS Altitude)

Assuming that the GPS satellites nominally are Earth-pointed and have a broadcast cone of ≈42.5^o, the visibility at high altitudes can be calculated by removing that portion of the RF cone that is blocked by the Earth (Figure 4.4). At GPS altitude, this amounts to 27.8^o of obscuration[33].

$$\theta = \cos^{-1}\left(-\widehat{R}_{GPS} \cdot \vec{r}_{\text{LOS}}\right) \tag{4.11}$$

where $\widehat{R}_{GPS}$ is the unit vector from Earth to the GPS satellite and $\overrightarrow{r}_{\text{LOS}}$ is the Line-of-Sight vector from the receiver to the GPS satellite under consideration. The GPS satellite is then visible when

$$27.8^o < \theta_{\text{visible}} < 42.5^o \tag{4.12}$$

4.3.1.2 Filter Regimes

Different filter regimes were established based on orbit altitude and number of GPS satellites tracked. All use the common information matrices

$$H_{GPS_i^x} = \begin{bmatrix} \vec{r}_{\text{LOS}_i^x} & 0 & 0 & 0 & 1 & 0 \end{bmatrix} \tag{4.13}$$

$$H_{RGPS_{i,j}^x} = H_{GPS_i^x} - H_{GPS_j^x} = \begin{bmatrix} (\vec{r}_{\text{LOS}_i^x} - \vec{r}_{\text{LOS}_j^x}) & 0 & 0 & 0 & 0 & 0 \end{bmatrix} \tag{4.14}$$

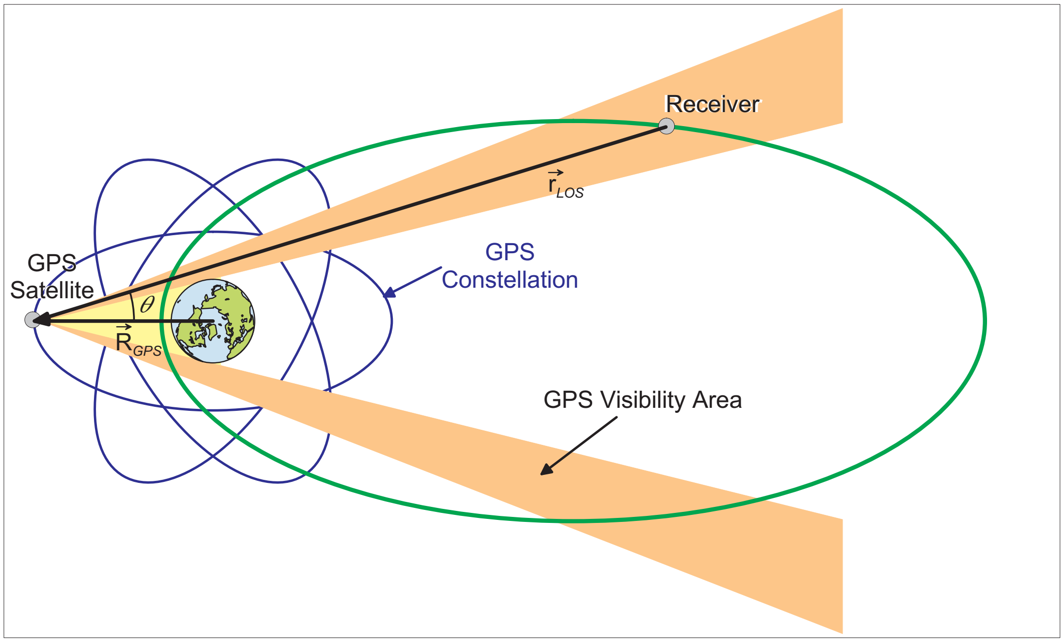

Figure 4.4: GPS Observability in the HEO Environment

where $\vec{r}_{\mathrm{LOS}_i^x}$ is the Line-of-Sight vector from formation member i to GPS satellite x.

1. *GPS Near*

When the formation is within three-quarters of the GPS altitude and two or more GPS satellites are tracked, the GPS-Near regime is used. Here RGPS can be performed on the formation to augment the code-based pseudorange measurements.

$$
\begin{aligned}
\widetilde{H}_{\text{GPS-near}} &= \begin{bmatrix} H_{GPS_1} & H_{RGPS_{1,2}} & H_{RGPS_{1,3}} & H_{RGPS_{1,4}} \end{bmatrix} \\
R_{\text{GPS-near}} &= \begin{bmatrix} (10\ m) & & \cdots & 0 \\ & (1\ m) & & \vdots \\ \vdots & & (1\ m) & \\ 0 & \cdots & & (1\ m) \end{bmatrix} \\
y_{GPS^x} &= R_{GPS^x} - (\rho_{GPS^x} + c\delta t) \qquad (4.15) \\
y_{RGPS^{x,y}_{1,j}} &= R_{GPS^x_1} - R_{GPS^y_1} - R_{GPS^x_j} + R_{GPS^y_j} - \rho_{RGPS^{x,y}_{1,j}} \\
y &= \begin{bmatrix} y_{GPS^1} & y_{GPS^2} & \cdots & y_{RGPS^{1,2}_{1,2}} & y_{RGPS^{1,3}_{1,2}} & \cdots \end{bmatrix}
\end{aligned}
$$

2. *GPS Far*

When the formation is outside the area of primary GPS availability, there is still signal availability through the RF spillover from GPS satellites on the far side of the Earth (Figure 4.4). The number of visible satellites will be limited, while the long signal path and lack of geometric distribution make RGPS ineffective.

$$
\begin{aligned}
\widetilde{H}_{\text{GPS-far}} &= \begin{bmatrix} H_{GPS} \end{bmatrix} \\
R_{\text{GPS-far}} &= 10\ m \\
y_{GPS^x} &= R_{GPS^x} - (\rho_{GPS^x} + c\delta t) \qquad (4.16) \\
y &= [\ y_{GPS^1}\ y_{GPS^2}\ \ldots]
\end{aligned}
$$

3. *Dead Reckoning*

When no GPS measurements are available, the measurement accumulation and update portion of the Kalman filter algorithm are skipped and the estimated state positions and covariance are propagated ahead to the next epoch. Because the knowledge of the system dynamics does not include the unmodelled perturbations described earlier in Section 4.2, large errors can be introduced by the time propagation step.

4.3.2 Transponder-Only Estimation

Another possibility for relative navigation of the formation is the use of a high-accuracy transponder measurement between formation members. This allows some precise navigation but removes the capability to align with an external time source.

$$\begin{aligned}
\widetilde{H}_{Transp} &= \left[\ (2\vec{r}_{LOS} + 4\delta t\vec{r}_{LOS})\ 0\ 0\ 0\ 0\ 0\ 0\ 2\rho/c\ \right] \\
R_{Transp} &= 10\ m \\
y_{Transp} &= \left(2R_{SATi} - 2\delta\dot{t}R_{SATi}\right) - \rho_{Transp} \qquad (4.17)
\end{aligned}$$

where

$$\begin{aligned}
\vec{r}_{LOS} &= \text{Line-of-Sight vector to other formation member} \\
R_{SATi} &= \text{Range to formation member } i
\end{aligned}$$

4.3.3 Transponder/GPS Estimation

Another possibility for relative navigation of the formation is the use of the high-accuracy, intersatellite transponder in conjunction with GPS receivers and a simple data exchange crosslink.

$$
\begin{aligned}
\widetilde{H}_{Combo} &= \left[\ H_{Transp}\ H_{GPS}\ H_{RGPS}\ H_{RGPS}\ H_{RGPS}\ \right] \\
R_{Combo} &= \begin{bmatrix} (10\ m) & \cdots & & & 0 \\ \vdots & (10\ m) & & & \\ & & (1\ m) & & \\ & & & (1\ m) & \vdots \\ 0 & & & \cdots & (1\ m) \end{bmatrix} \\
y_{Combo} &= \left[\ y_{Transp}\ y_{GPS}\ y_{RGPS_{1,2}}\ y_{RGPS_{1,3}}\ y_{DPGS_{1,4}}\ \right]
\end{aligned} \tag{4.18}
$$

The new measurement types are incorporated by "stacking" the measurement and noise matrices with the additional data type. By example, this demonstrates how to append new measurement types to an existing filter to perform sensor fusion.

4.3.4 Simulation/Estimation Assumptions

There were several assumptions made in design of the estimator and simulation which are worth noting before examining the results. In all cases where carrier phase range measurements were used, sensor accuracies were reported for these cases assuming that the integers had been properly resolved. There are a wide range of techniques for resolving phase integers, and each have varying efficacy in different environments [32], [25], [37]. In addition, no simulation or allowance is made for multipath at the receiving antenna. This will vary greatly depending upon the size and geometry of the chassis itself, so these errors are left to the individual mission designer to consider. More information on these techniques is presented in Kaplan[25] and Hofmann[23].

4.4 HEO Results

All results presented are from the perspective of a single spacecraft (number 1 in Figure 4.2), as if the navigation filters are executing on board that particular spacecraft. A true relative trajectory about the reference orbit is computed as part of the simulation, and the error results presented are deviations from that computed true trajectory. It is assumed that each member of the formation will be performing this task and exchanging estimated state information in the process. A very important consideration that is not detailed here is time synchronization. Accurate relative navigation depends upon the ability to compare timed measurements within the formation and with external references. Dynamic models often depend on accurate time synchronization as well. Time biases are presented here as estimated state errors but are not shown for their contribution to the navigation error.

4.4.1 GPS-Only Navigation

As discussed in Section 4.3.1, the first case uses only on-board GPS and a simple data-exchange crosslink to perform differential GPS when visibility allows. Figure 4.5 shows the relative navigation errors over four orbit periods, beginning at apogee. There are noticeably large outlying measurements, up to and exceeding 2 kilometers, especially during periods with little or no signal availability. Here the navigation filter can only perform dead-reckoning in the presence of unmodelled perturbations. Near perigee, the formation enters a measurement-rich environment and the filter converges rapidly. A closer view is shown in Figure 4.6, where the brief region of full GPS coverage is seen to give performance errors of around 1 meter. These errors are consistent with the LEO GPS-only results shown in Section 3.5.2.

It is interesting and informative to see where the relative navigation performance is poorest and best, especially as it relates to the number of visible GPS satellites. Figure 4.7 shows the combined 3-axis error on the same plot with GPS visibility, and as a general trend the filter performance seems to improve with the number of visible satellites. Also of note in the filter performance is the ability to correctly model and track the clock bias generated by the oscillator random walk. The typical oscillator parameters defined in Section 2.2 were used. Figure 4.8 shows this error, and several large diversions are noticeable up to and exceeding 100 milliseconds. Figures 4.9 and 4.10 show the actual relative trajectory computed by the navigation filter. It is clear that many of the larger errors occur near apogee, as is expected when signal reception is often poorest.

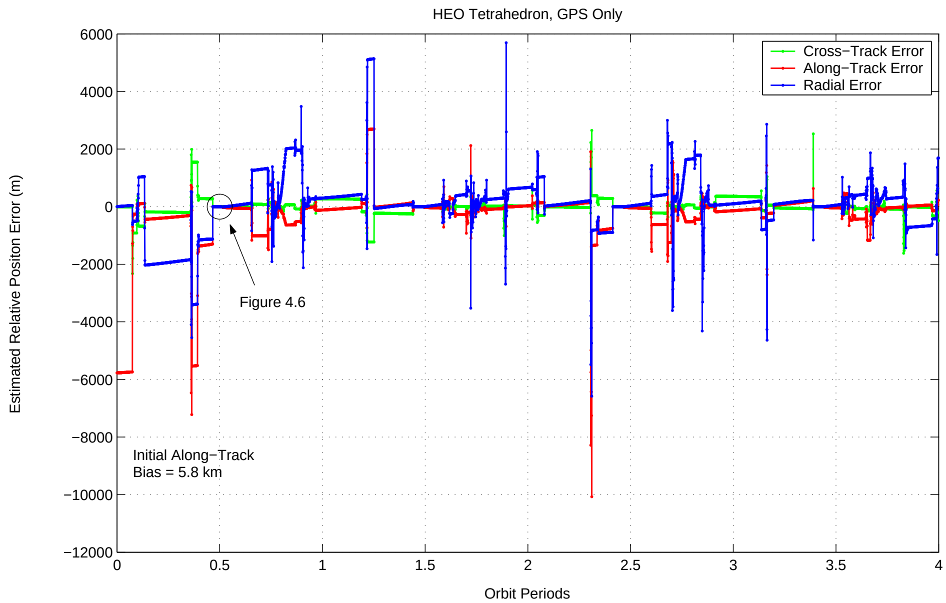

Figure 4.5: GPS Only, Relative Navigation Errors

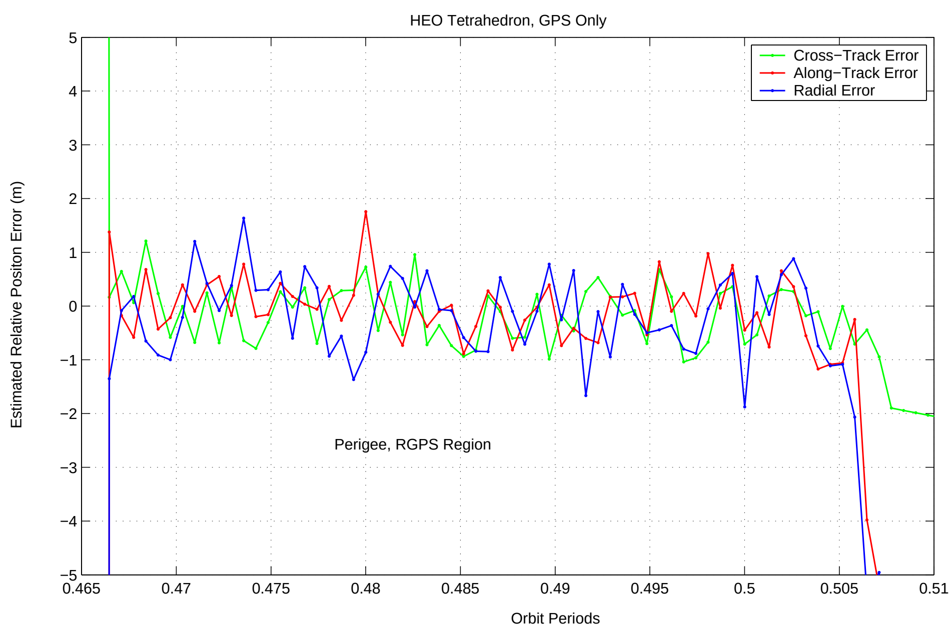

Figure 4.6: GPS Only, Relative Navigation Errors (Zoomed View)

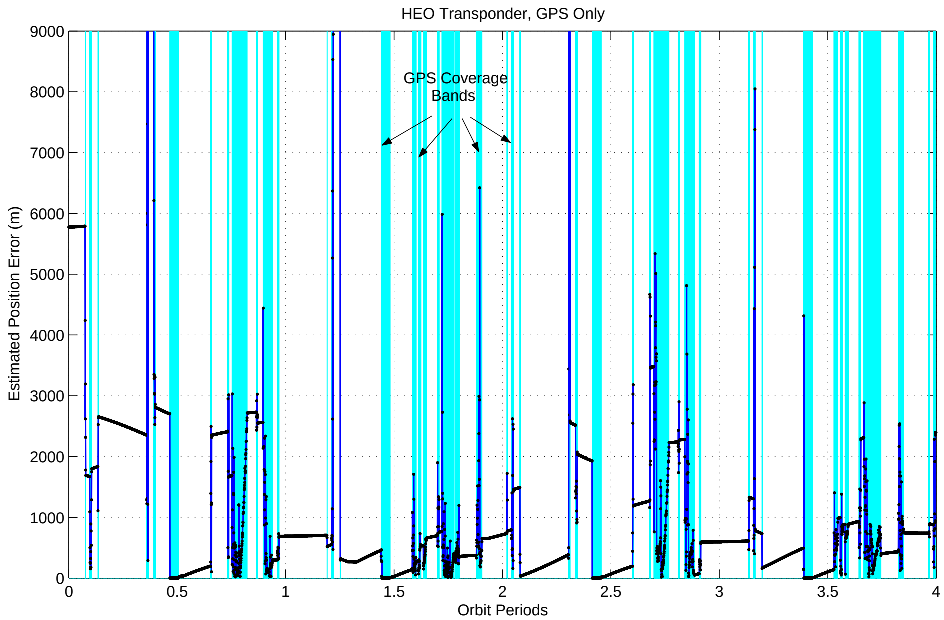

Figure 4.7: GPS Only, Combined 3-Axis Error shown with GPS Availability

Figure 4.8: GPS Only, Estimated Clock Bias Error

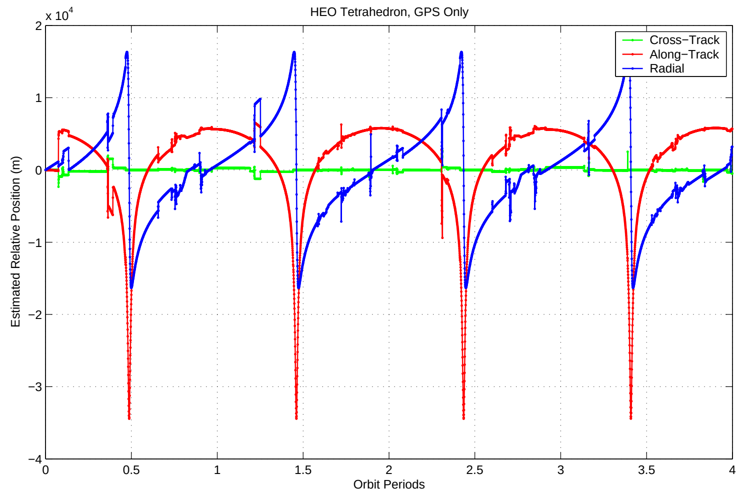

Figure 4.9: GPS Only, Relative Position Estimate Components

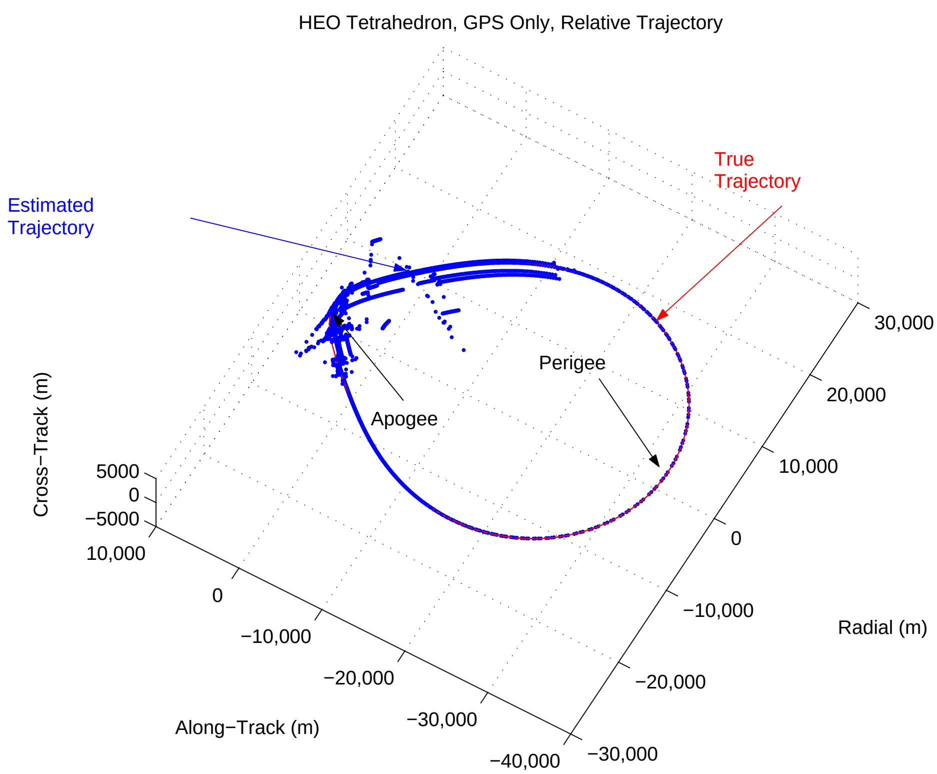

Figure 4.10: GPS Only, Estimated Relative Trajectory for Satellite 1

4.4.2 Transponder-Only Navigation

Another sensor possibility is to only use on-board intersatellite transponders, given some initialization by GPS or DSN and then only tracking other members of the formation thereafter. Unlike the GPS-only case, the signals are always present and no dead-reckoning is required. However, the small size and relative proximity of the formation can lead to geometric distribution problems. In addition, there is no external time reference for the formation so any time-tagged data will be subject to timing errors pursuant to the estimated clock bias error of the filter. An alternative would be to allow one formation member to have a "master clock" which keeps formation time. Finally, the transponder does not provide absolute position knowledge, which is necessary to propagate the system equations of motion.

The relative position error estimates for the transponder-only case are shown in Figure 4.11. It is seen that the filter converges quickly from an initial bias. Large cross-track errors are obvious at particular locations in the estimate. These regions correspond to the locations where the formation becomes planar, losing all geometric distribution in the cross-track axis. There are radial and along track errors on the order of a few meters, while cross-track errors can exceed 20 meters in the worst case geometries. A closer examination of this cross-track error is shown in Figure 4.12, where the cross-track DOP confirms the location where the formation becomes planar and geometric distribution along that axis is lost. Clock estimator performance is shown in Figure 4.13. Errors are seen to be in the 100 to 200 microsecond range, but grow larger as time elapses. This is expected since there is no absolute time reference and thus no way to observe and correct clock drift. The estimated relative trajectory is shown in Figures 4.14 and 4.15. It is notable that, unlike the GPS-only case, errors at apogee are comparable to those at perigee.

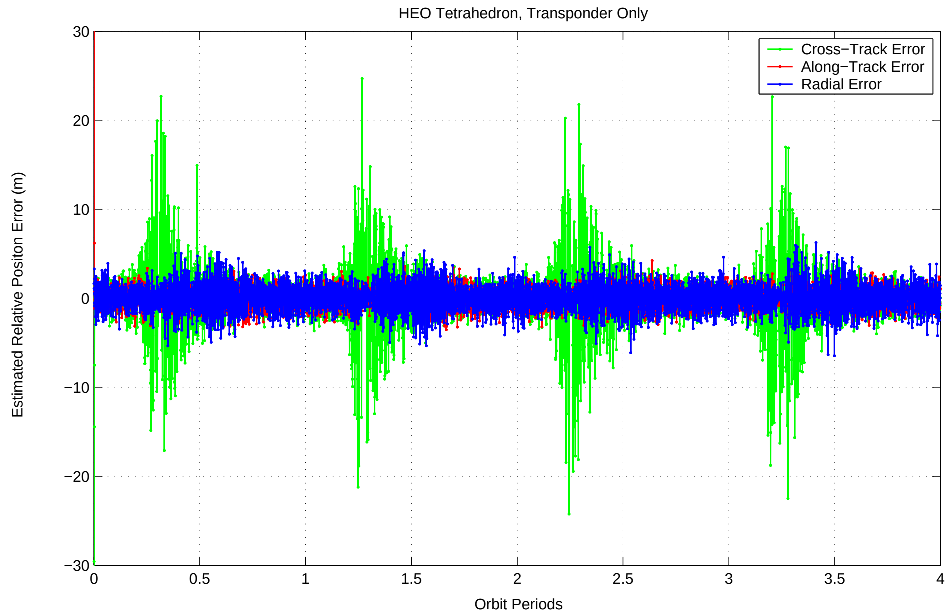

Figure 4.11: Transponder Only, Relative Navigation Errors

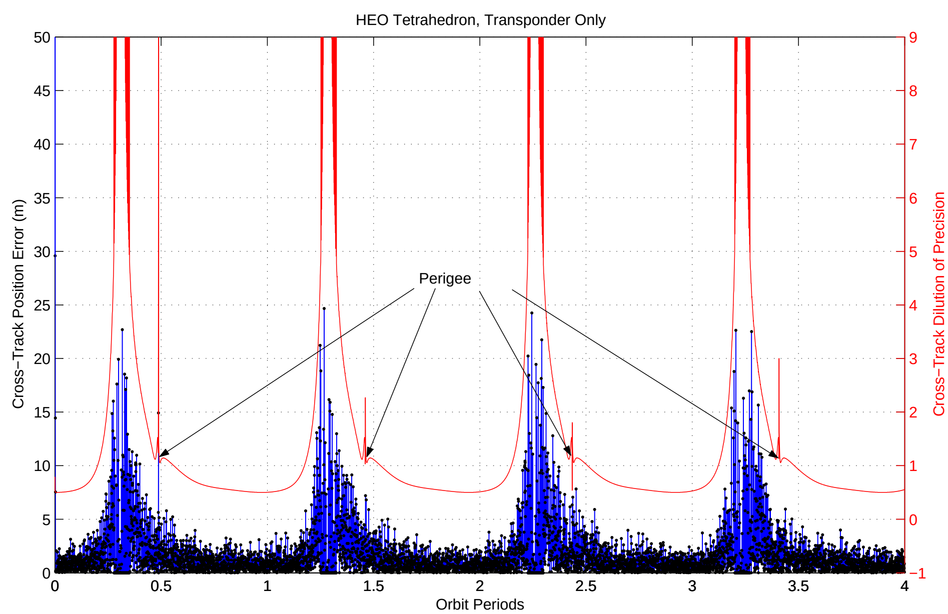

Figure 4.12: Transponder Only, Cross-Track Navigation Errors and DOP

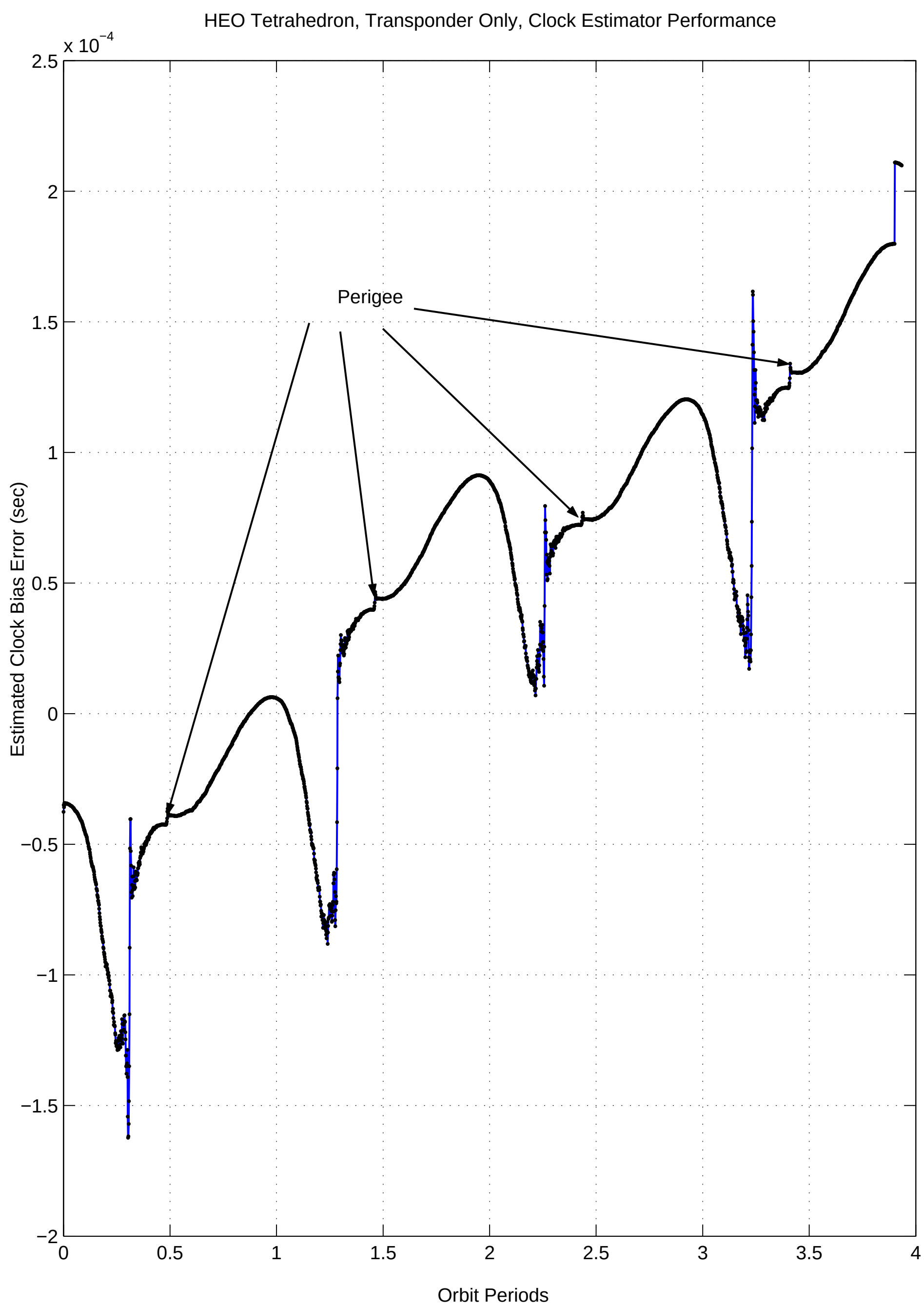

Figure 4.13: Transponder Only, Estimated Clock Bias Error

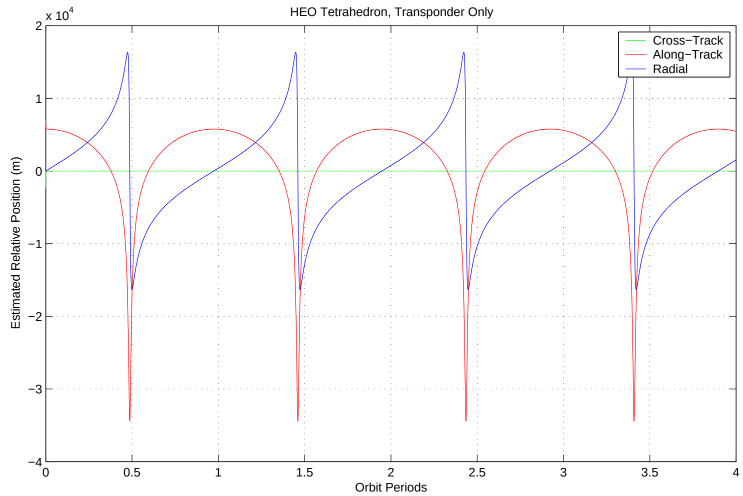

Figure 4.14: Transponder Only, Relative Position Estimate Components

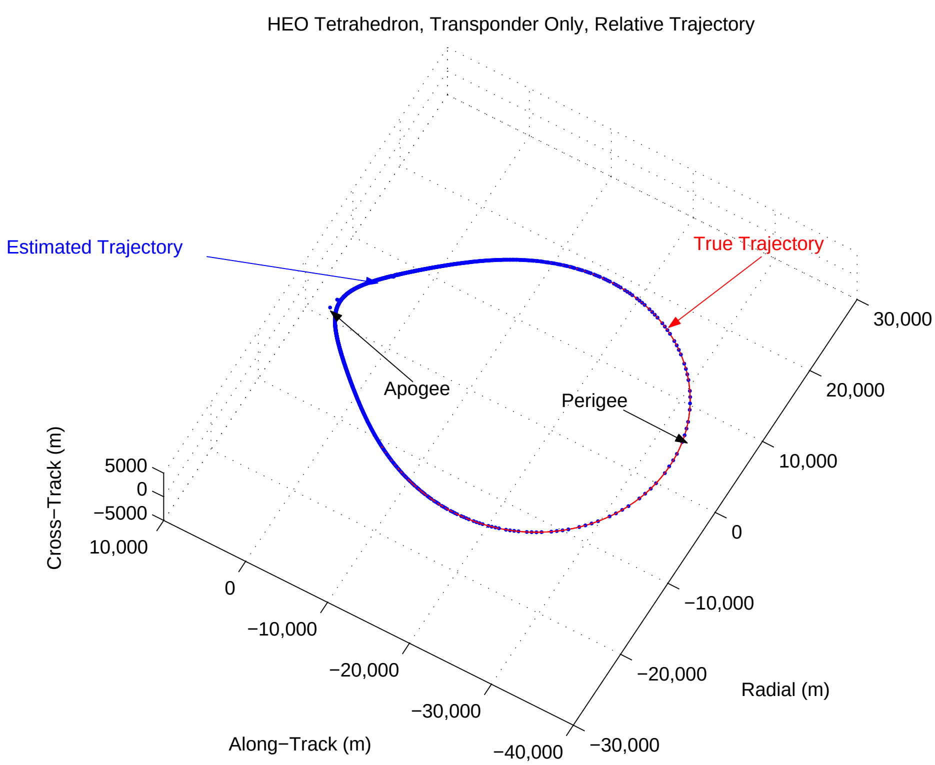

Figure 4.15: Transponder Only, Estimated Relative Trajectory for Satellite 1

4.4.3 Transponder/GPS Navigation

To overcome the shortcomings of the previous methods, a combined sensor suite may be used with a transponder system providing precise ranging while GPS supplements with precise timing and differential corrections as visibility allows. This also provides an external time reference to facilitate precise tagging of data collected by the formation and curtail long-term drift of the clock from absolute time.

The estimated relative position errors for the combined transponder/GPS case are shown in Figure 4.16. As in the transponder-only case, convergence occurs quickly. A closer view in Figure 4.17 shows that the combined sensor filter is also subject to cross-track errors at the points where the formation becomes planar. This would suggest that singular geometries should be avoided when designing formations. There are not sufficient GPS measurements in these areas to remove the associated errors. The view clearly shows the region where the measurement-rich LEO environment allows the RGPS portion of the filter to drive errors to less than 1 meter. This performance is superior to the transponder-only system in this region. As in the transponder-only case, an examination of the cross-track error displays the inherent weakness of the filter when formation geometry is poor. A striking difference from all previous cases is seen, however, when the clock bias error estimate is examined in Figure 4.18. The transponder portion of the filter keeps outliers to a minimum, while the GPS portion updates and aligns the filter with the external time source. A closer view in Figure 4.19 shows these realignments occurring. Dur-

Table 4.3: Root-Mean-Square Error over Four Orbit Periods

Sensor Type	Radial (m)	Along-Track (m)	Cross-Track (m)
GPS Only	972.87	1032.4	268.44
Transponder Only	1.4050	0.9679	2.8685
Combined	1.3748	0.9502	2.9376

Table 4.4: Root-Mean-Square Error at Perigee

Sensor Type	Radial (m)	Along-Track (m)	Cross-Track (m)
GPS Only	1.2083	1.0016	0.5601
Transponder Only	1.6720	1.0107	3.0691
Combined	0.7818	0.5860	0.5378

ing the measurement-rich region close to perigee, accuracies of 50 nanoseconds or better are seen.

The results of the simulation studies are shown in Table 4.3 and Table 4.4 . It is notable that the combined sensor type shows the best performance in most of the cases considered.

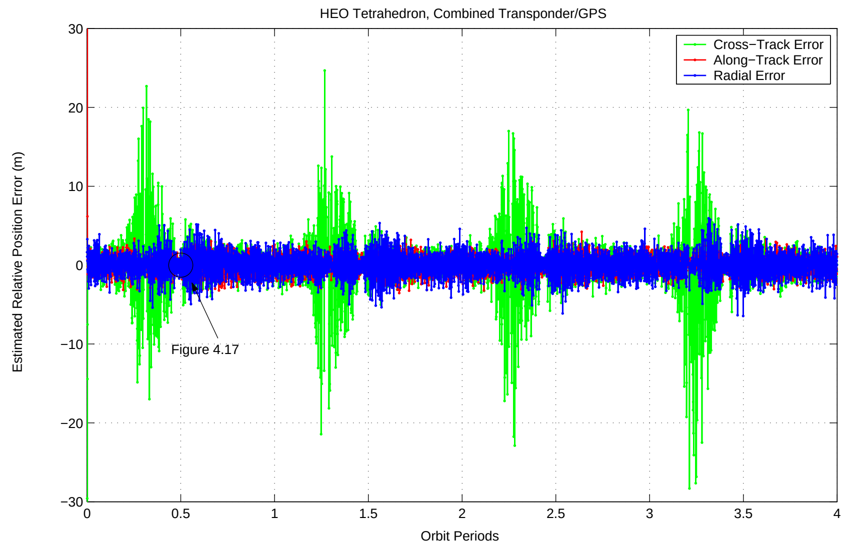

Figure 4.16: Combined Transponder/GPS, Relative Navigation Errors

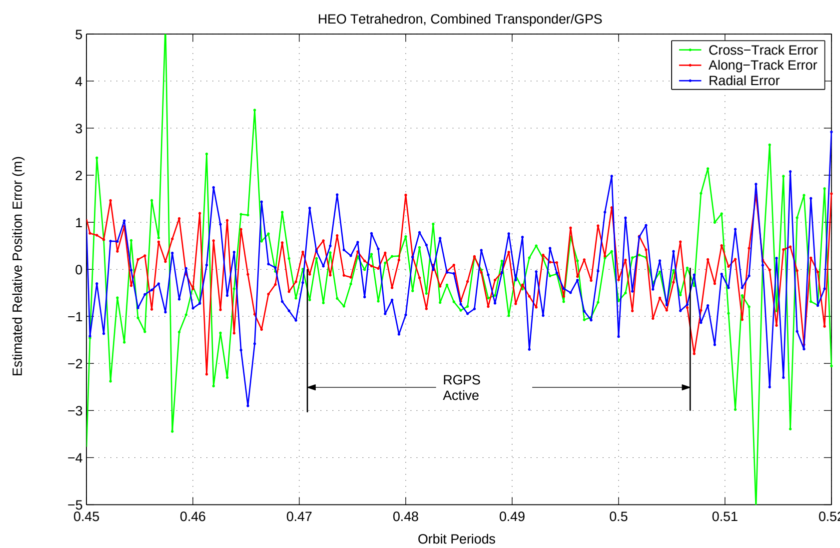

Figure 4.17: Combined Transponder/GPS, Relative Navigation Errors (Zoomed View)

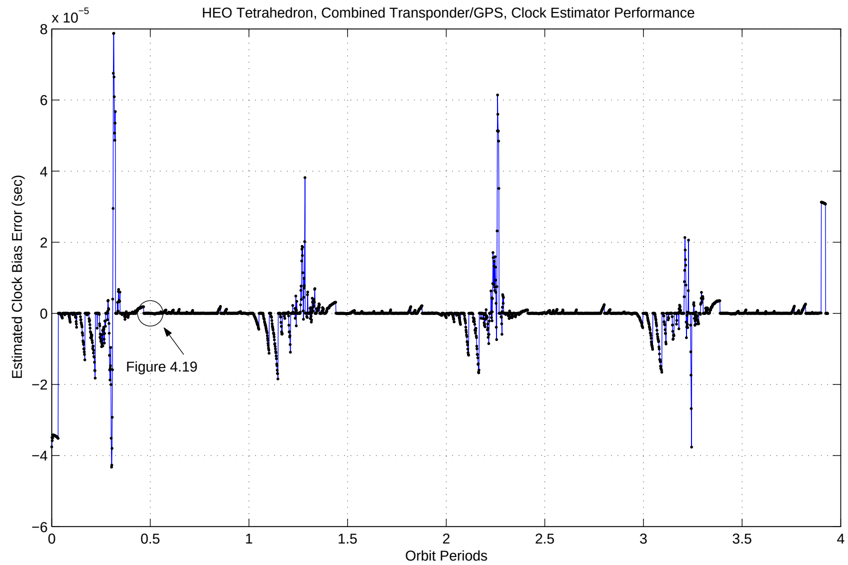

Figure 4.18: Combined Transponder/GPS, Estimated Clock Bias Error

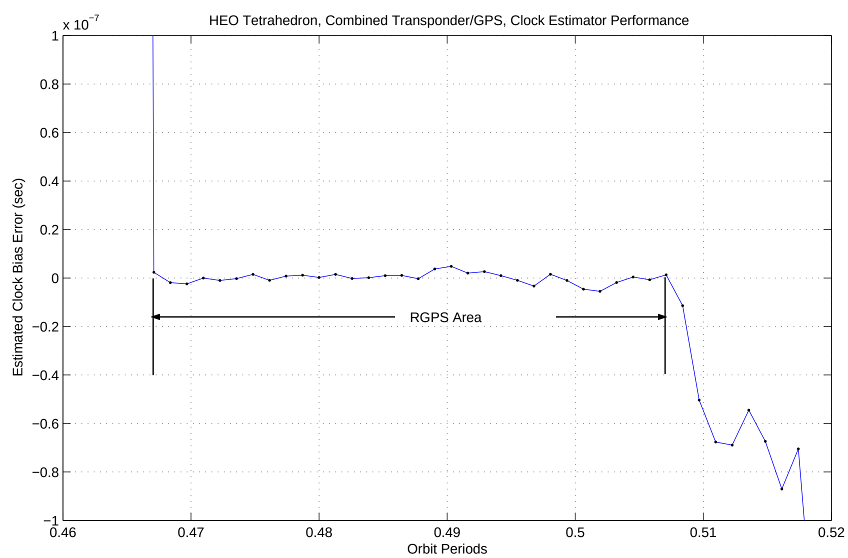

Figure 4.19: Combined Transponder/GPS, Estimated Clock Bias Error (Zoomed View)

Chapter 5

Libration Point Orbit

In the restricted problem of three bodies, there are five points in the plane of motion where the gravitational forces of the two attracting bodies are balanced, described in detail by Szebehely and Mark [41]. Three of these libration points are colinear with the attracting bodies, while two are located at the vertex of an equilateral triangle formed by the attracting bodies. This configuration can be seen in Figure 5.1. A spacecraft can travel a semi-repeating trajectory about a libration point known as a Lissajou Orbit (Figure 5.2). When a collection of these satellites all travel slightly offset Lissajou orbits about the libration point, they can be arranged into a formation. A satellite formation in an orbit about a Sun-Earth libration point is of interest to many mission designers. Formations in these orbits may be used as large baseline interferometers for deep-space observation. Their distance from the Earth, around 1.5 million km, gives an observation environment with minimal radio interference. A mission of this type is baselined in Carpenter, et al. [11] for use as a reference.

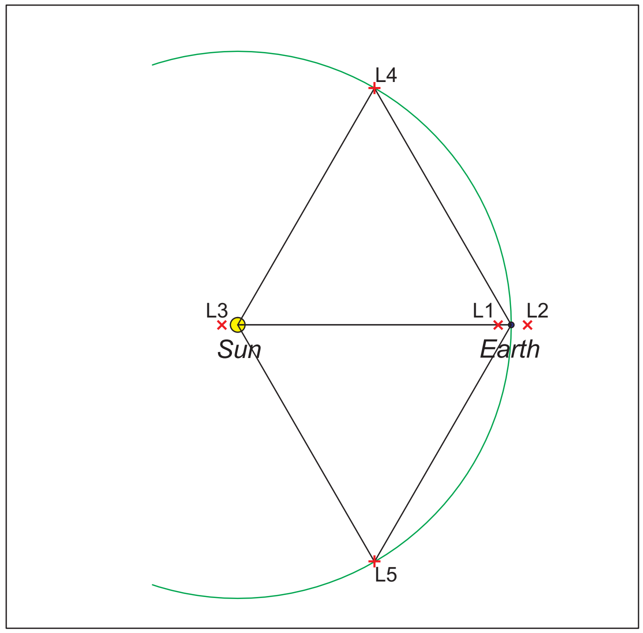

Figure 5.1: Libration Points for Sun/Earth System (not to scale)

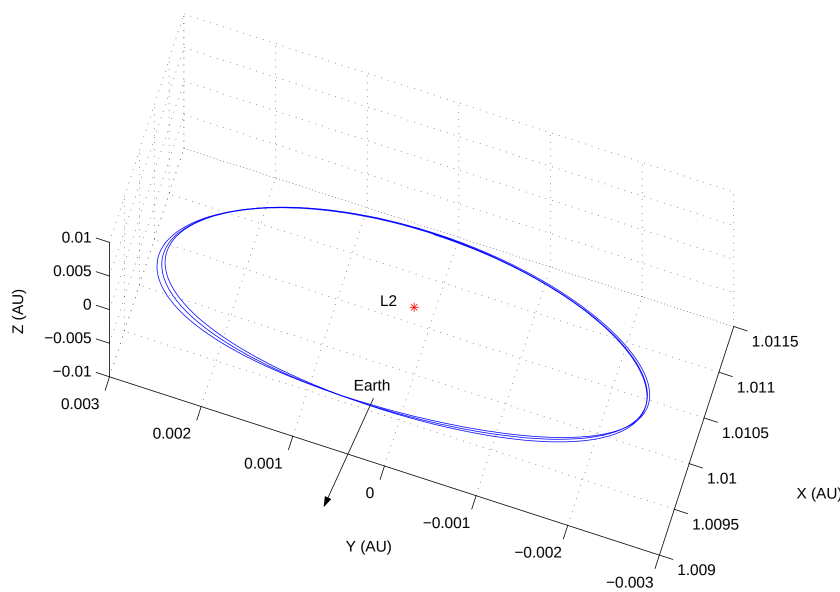

Figure 5.2: Lissajous Orbit about L2 Libration Point

5.1 Libration Challenges

There are additional challenges with formation navigation about a libration point. The relative equations of motion are very different than a LEO or HEO orbit. The orbit location is also outside the coverage of GPS, so relative navigation must be accomplished almost exclusively with on-board sensors. The formation geometry is much slower changing that LEO or HEO.

5.2 Libration Simulation

The formation that was simulated for this study was based upon the libration benchmark orbit suggested by Carpenter [11]. This study, like the HEO simulation, was performed as an example of many typical applications. Again, the sensor models developed in the previous chapters were implemented into a MATLAB simulation of Lissajou orbit dynamics. The reference orbit is shown in Figure 5.3. It involves a 300,000 km Lissajou orbit about the trans-terrestrial libration point, labelled "L2" in Figure 5.1. The formation itself makes up an aspherical surface about the reference orbit with a radius of 250 m. This formation configuration is shown in Figure 5.4. The relative trajectories that this configuration produces are shown in Figure 5.5.

5.3 Equations of Motion

The libration point orbit is an artifact of the restricted problem of three bodies. It is often derived in terms of a rotating reference frame containing the

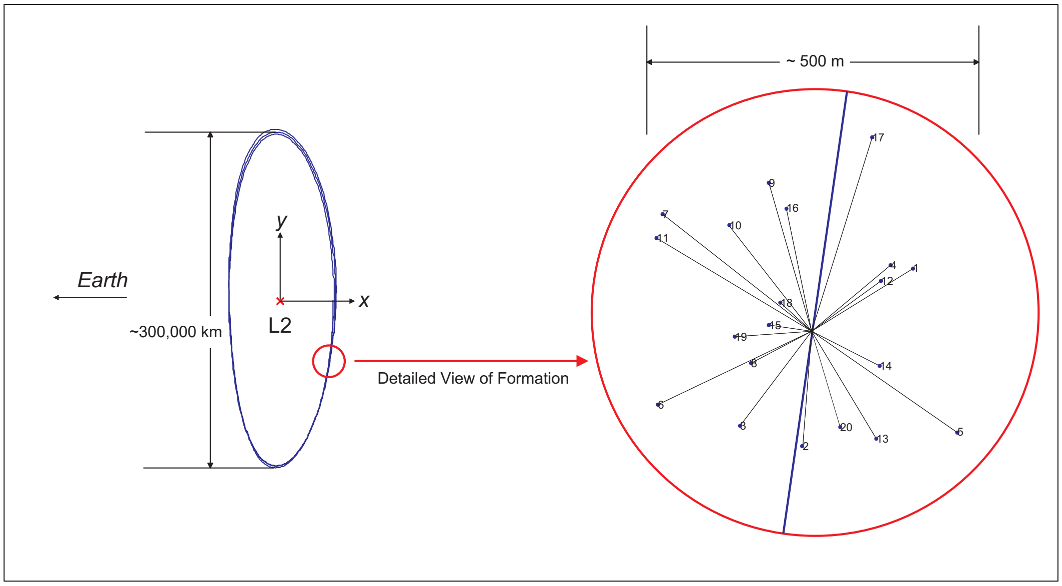

Figure 5.3: Aspherical Formation about L2 Lissajous Orbit

primary bodies and normalized to the distance between them. It is described by the following equations of motion[45]:

$$\begin{aligned}
\ddot{x} &= x + 2\dot{y} - \frac{1-\mu}{r_1^3}(x+\mu) - \frac{\mu}{r_2^3}(x-1+\mu) \\
\ddot{y} &= y - 2\dot{x} - \frac{1-\mu}{r_1^3}y - \frac{\mu}{r_2^3}y \\
\ddot{z} &= -\frac{1-\mu}{r_1^3}z - \frac{\mu}{r_2^3}z
\end{aligned} \tag{5.1}$$

where

$$\begin{aligned}
\mu &= \text{mass ratio of the restricted three-body problem} \\
r_1 &= \sqrt{(x+\mu)^2 + y^2 + z^3} \\
r_2 &= \sqrt{(x-1+\mu)^2 + y^2 + z^3}
\end{aligned}$$

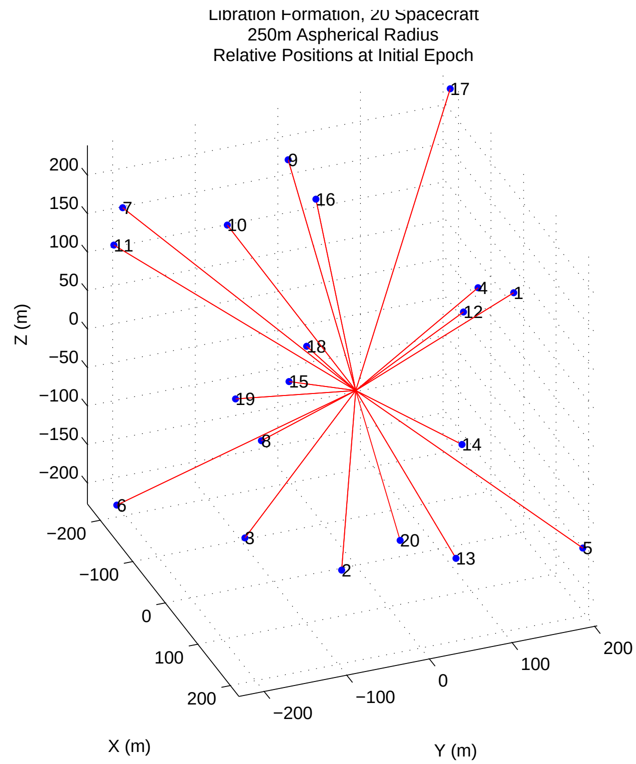

Figure 5.4: Relative Positions about Reference Lissajous orbit

These equations of motion give the Lissajou orbit shown in Figure 5.2, while small variations in the initial conditions give rise to the relative trajectories in Figure 5.5.

5.4 Estimation Technique

The estimation technique employed for the libration simulation was very similar to that used in the Transponder-Only HEO case. The number of measurements, though, was much higher (19 vs. 3) so the size of the information and measurement matrices was adjusted accordingly. In addition, the

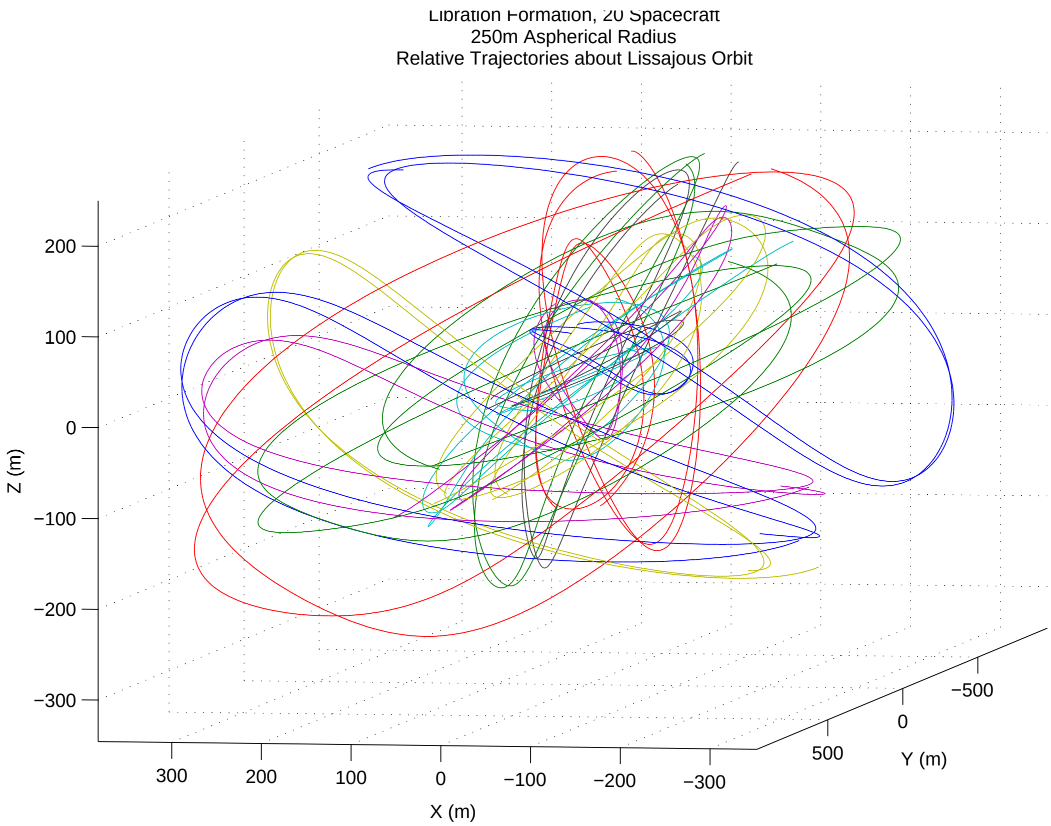

Figure 5.5: Relative Trajectories about Reference Lissajous Orbit

equations of motion used for the prediction routine of the EKF were changed to match the Lissajou orbit dynamics.

5.5 Libration Results

As in the HEO case, it was assumed for this study that the phase measurements are taken with integers properly resolved. All results presented are from the perspective of a single spacecraft (number 1 in Figure 5.4), as if the navigation filters are executing on board that particular spacecraft. As in the

HEO case, it is assumed that each member of the formation will be performing this task and exchanging estimated state information in the process. With 20 evenly distributed spacecraft in the formation, there are no geometric distribution problems as in the 4 spacecraft HEO case. Since all the relative navigation is self-contained in the formation, all timing information must be derived from oscillators aboard the spacecraft. The only exception is occasional contacts with an Earth station such as NASA's Deep Space Network (DSN). This allows coarse initialization of the formation and time synchronization capabilities.

Figure 5.6 shows the relative position error of the EKF. The DSN ranging is able to provide some coarse initial formation knowledge, within about a kilometer along the Earth line-of-sight direction but only to within tens of kilometers out of plane [7]. Because of the coarse initial knowledge and the very slow geometry changes of this formation, the filter convergence takes longer that the LEO or HEO case. It is seen that the filter takes almost a full day to reach a converged navigation solution. Once converged, however, the relative positioning error remains less than 10 cm. The relative velocity error is shown in Figure 5.7. The convergence time is similar to that of the relative position, taking about a full day. Once converged the errors remain less than 2 m/s. Figure 5.8 shows the clock drift errors in the EKF. The clock is derived from the random walk model described in the previous chapters, and without an external reference the errors grow without bound. The error grows at a rate of about 6 ms/day and would affect the time-tag of any data generated by this spacecraft. The estimated clock drift is shown in Figure

5.9. Since the transponder measurement is heavily dependent upon the clock drift, the filter tracking performs well. After convergence, errors were around 2-3 ns/s. Finally, the trajectory is shown in Figure 5.10. It is seen that the solution estimate converges from a coarse initial state onto the true trajectory and continues to track well.

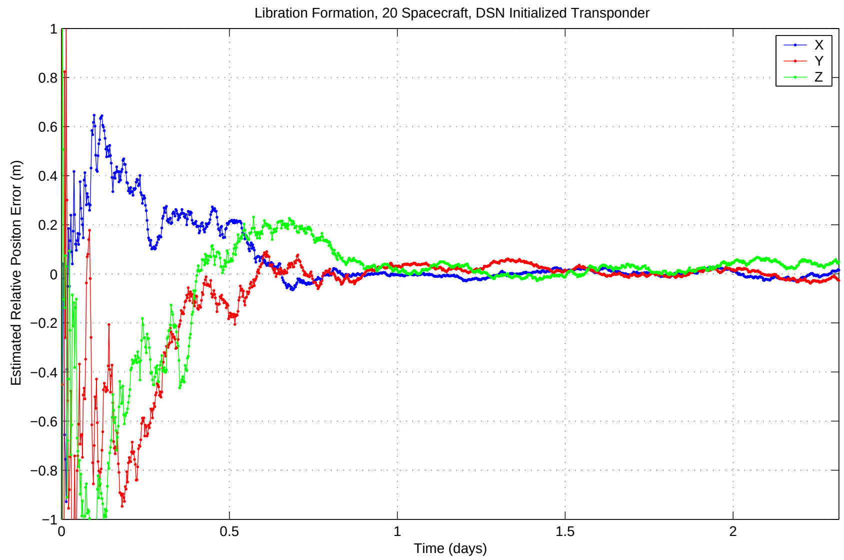

Figure 5.6: Estimated Relative Position Error

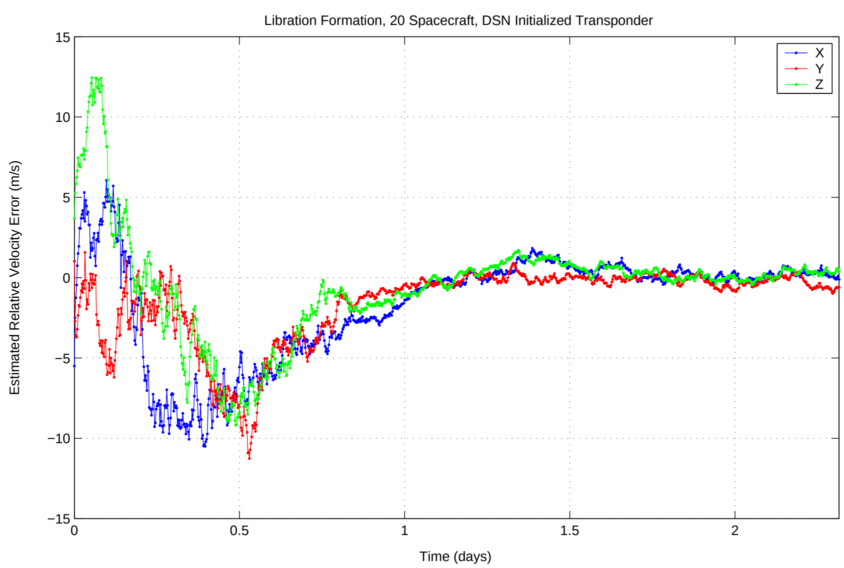

Figure 5.7: Estimated Relative Velocity Error

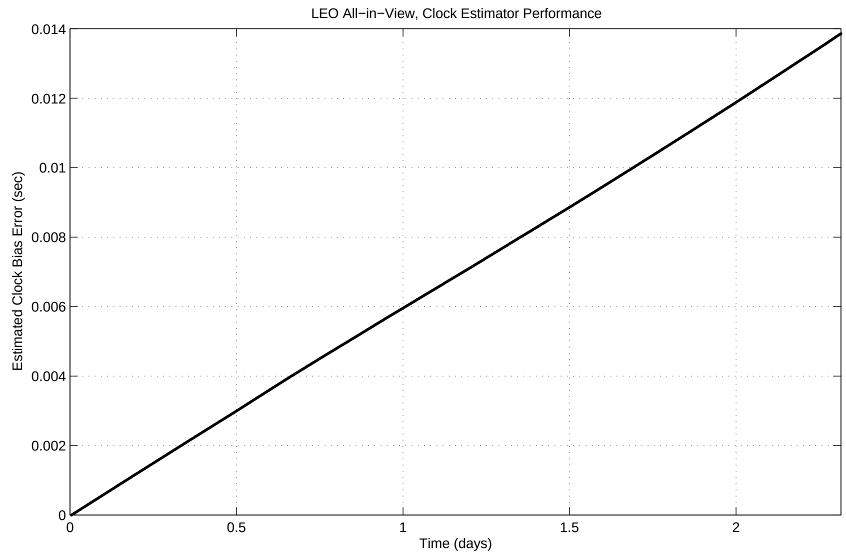

Figure 5.8: Estimated Clock Bias Error (d_0)

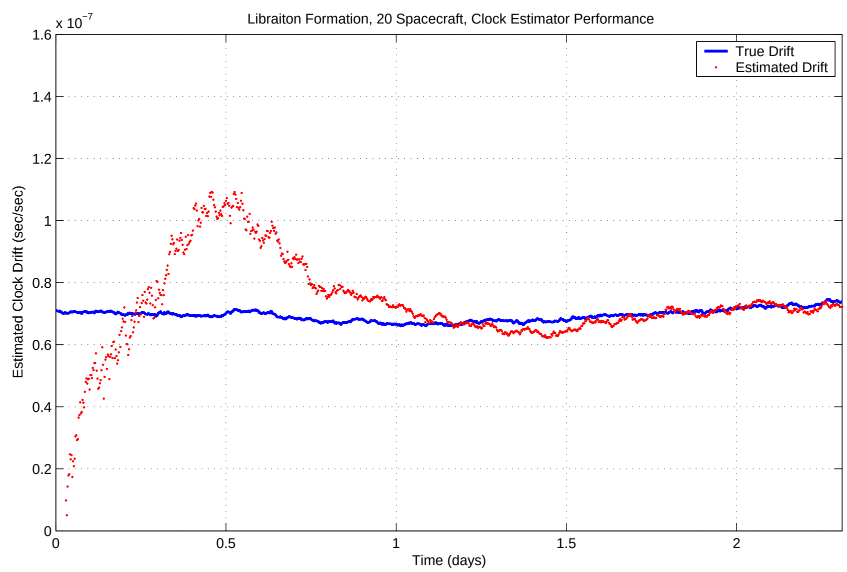

Figure 5.9: Estimated Clock Drift (a_0)

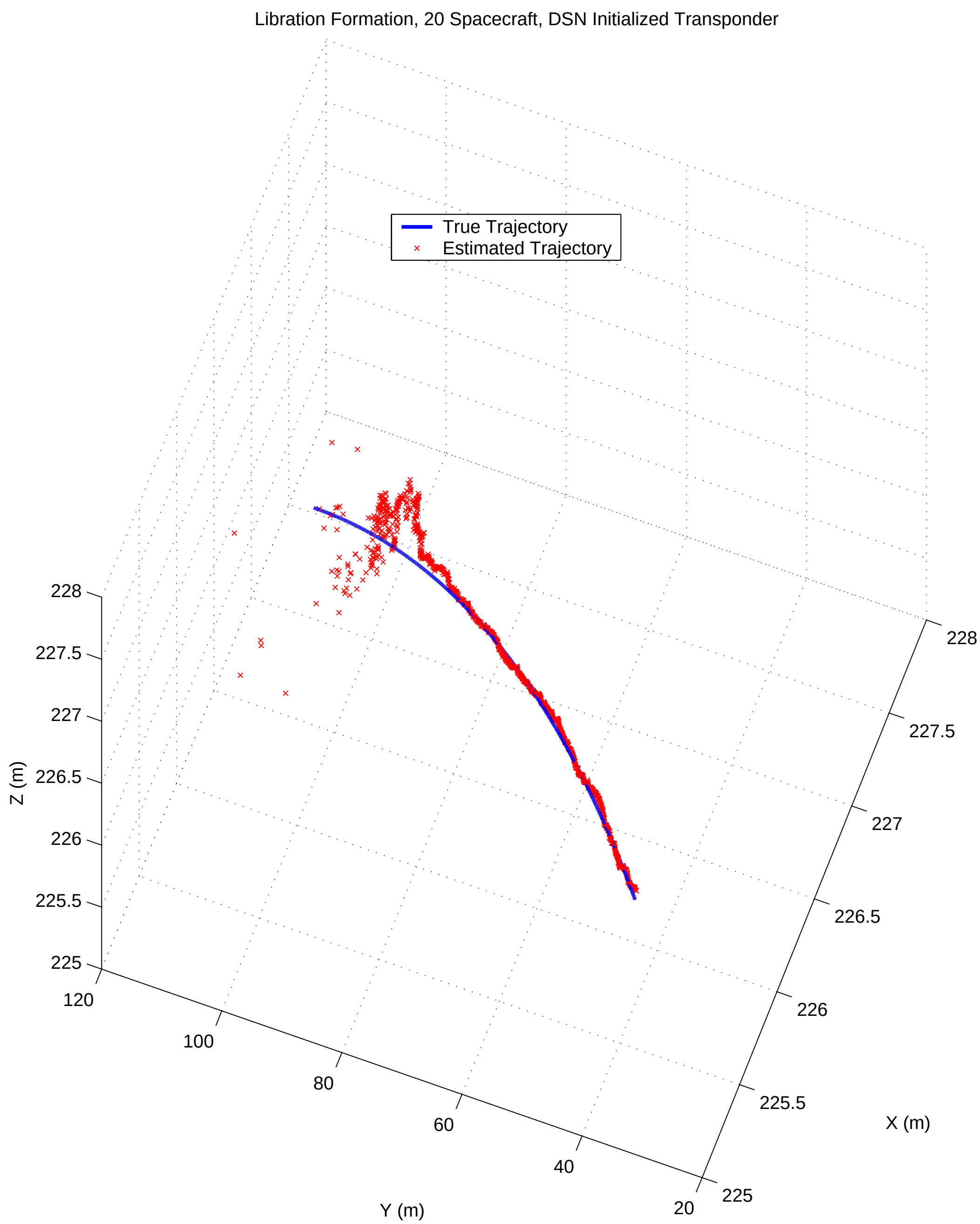

Figure 5.10: Estimated Trajectory of Spacecraft 1

Chapter 6

Conclusions

The objective of this dissertation was to investigate the modelling, combining, and applying of sensor ranging measurements in a relative positioning algorithm. Mission designers can use these to incorporate multiple sensors, compare filter performance, and analyze noise sources. This chapter provides a summary of the contributions, as well as discussion of future work in the area of formation flying sensor analysis.

6.1 Summary of Research Contributions

This dissertation makes the following contributions to the field of satellite formation flying.

6.1.1 LEO Microsatellite Sensor Development

A LEO formation flying sensor that utilized multiple measurement inputs was developed into a flight-ready unit for use aboard the FASTRAC nanosatellite. An EKF was utilized which combined GPS SNR measurements with magnetometer field measurements to estimate the vehicle attitude. This is an example of the integration of multiple measurements using a generalized technique. Hardware simulation results show attitude determination accuracies to within 10 degrees using this technique.

6.1.2 Sensor Measurement Models

Generalized sensor models were developed for transponder measurement types which are of the same general form as traditional one-way measurement equations. Using time-of-flight ranging principles, these models are more easily adapted to simulation and analysis because of their familiar nature. It is believed that this is the first time that this measurement type has been presented in a form conducive to its inclusion in existing relative navigation filters.

6.1.3 Error Characteristics

The incorporation of error sources into the sensor measurement models was another contribution of this dissertation. The error models were constructed from actual measured sensor noise characteristics where available. Different formation environments were simulated using the same noise and error models, allowing for accurate comparison between them.

6.1.4 HEO/Libration Orbit RelNav Filters

Navigation filters were presented for formations in HEO and libration point orbits. These filters incorporated the sensor models derived in the earlier chapters. In the HEO case, three different measurement combinations are presented. When a combination of GPS and transponder measurements were used, the estimator performance was improved. This was especially noticeable at perigee, where errors were reduced from 1.6 to 1.1 meters when the combined sensor filter was used. In the libration orbit case, the filter design incorporated the dynamics of that environment to give relative navigation performance at the level of 10 *cm* with up to day-long convergence times.

6.1.5 Sensor Fusion

A generalized approach for incorporating multiple sensor types into a navigation filter is presented. First, the measurement is expressed in a form that is easily incorporated with the other sensors. Next, the EKF filter equations are augmented with a model of the additional sensor. Examples were given for combined sensor algorithms. The first of these was an attitude determination filter that incorporates GPS SNR and magnetometer measurements in the same filter. The other example is combined GPS/Transponder filter for use in HEO. In both cases, the additional sensor information aids the filter in accuracy and/or robustness.

6.1.6 Applications

A progression is shown for applications of various measurement types in different formation flying environments. First, the LEO case is considered and the FASTRAC microsatellite sensor is described. A LEO simulation is also performed using the readily available GPS measurements present in that environment. Next, the HEO case is considered, and a simulation produced using the same error and measurement models. Several different sensor types are considered and shown, including a combined sensor filter using GPS and localized transponder measurements. Finally, the progression is extended to an orbit about the Earth/Sun libration point where GPS measurements are unavailable. The filters incorporate the same measurement models but have dynamic models that reflect the libration point orbit environment.

6.2 Suggestions for Future Work

There is much opportunity to build upon this research and further examine the topic of spacecraft formation flight. Integer ambiguity techniques and multipath modelling were deliberately excluded from this study as being too mission specific, but could be implemented if exploring a particular formation application. The estimated state could also be examined for elements to add or remove. For example, the clock bias term could be removed from a transponder-only filter and the spacecraft clock propagated from the clock drift estimate. Additional inter-formation sensors such as optical ranging devices could be modelled and incorporated into the filter routines. In addition, ground tracking could be included as an additional sensor measurement using the same combinatorial techniques shown in previous chapters. Relative formation attitude determination was also not considered in this study, but is important to many formation flying missions.

Sensor and dynamics models could be further refined for specific missions or perturbation environments. In addition, formation design work could be performed with sensor considerations in mind. By avoiding unfavorable formation geometries that lead to high DOP, the relative navigation filter errors can be improved.

Bibliography

[1] Alonso, R., J.L. Crassidis, and J.L. Junkins. Vision-Based Relative Navigation for Formation Flying of Spacecraft. In *Proceedings of the AIAA GNC Conference and Exhibit*, Denver, CO, August 2000.

[2] Alonso, R., J.Y. Du, D. Hughes, and J.L. Junkins. Relative Navigation for Formation Flying of Spacecraft. In *Proceedings of the NASA Goddard Space Flight Mechanics Symposium*, Greenbelt, MD, June 2001.

[3] Aung, M., et al. Autonomous Formation-Flying Sensor for the StarLight Mission. *IPN Progress Report*, 42-152, February 2003.

[4] Axelrad, P., and C.P. Behre. Satellite Attitude Determination Based on GPS Signal-to-Noise Ratio. *Proceedings of the IEEE*, Vol. 87(No. 1):pp. 133–144, January 1999.

[5] Bauer, F., et al. Enabling Spacecraft Formation Flying Through Spaceborne GPS and Enhanced Automation Technology. *Presented at the ION-GPS Conference*, September 1999.

[6] Bauer, F.H., J. Bristow, D. Folta, K. Hartman, D. Quinn, and J.P. How. Satellite Formation Flying Using an Innovative Autonomous Control System (AUTOCON) Environment. *Presented at the American Institute of*

Aeronautics and Astronautics (AIAA) Guidance, Navigation, and Control Conference, May 1997.

[7] Beckman, M. Orbit Determination Issues for Libration Point Orbits. *Proceedings of the International Conference on Libration Point Orbits and Applications*, June 2002.

[8] Broucke, R. Solution of the Elliptic Rendezvous Problem with the Time as Independent Variable. *Journal of Guidance, Control, and Dynamics*, Vol. 26(No. 4):pp. 615–621, July 2003.

[9] Buist, P.J., et al. Spacecraft Full Attitude Determination from a Single Antenna: Experimentation with the PoSAT-1 GPS Receiver. *Proceedings of the ION National Technical Meeting*, pages pp. 181–187, September 1998.

[10] Busse, F. Demonstration of Adaptive Extended Kalman Filtering for LEO Formation Estimation using CDGPS. *Journal of the Institute of Navigation*, Vol. 50(No. 2):pp. 79–94, Summer 2003.

[11] Carpenter, J. R., et al. Benchmark Problems for Spacecraft Formation Flying Missions. *Presented at the AIAA GNC Conference*, August 2003.

[12] Corazzini, T. *Onboard Pseudolite Augmentation for Spacecraft Formation Flying*. PhD thesis, Stanford University, August 2000.

[13] Curtis, S. The Magnetospheric Multiscale Mission... Resolving Fundamental Processes in Space Plasmas. *NASA/TM2000-209883*, December 1999.

[14] Das, A., and R. Cobb. TechSat21 - Space Missions Using Collaborating Constellations of Satellites. *Presented at the 12th Annual AIAA/USU Conference on Small Satellites*, (SSC98-VI-1), 1998.

[15] Dunn, C., and C. Duncan. Estimating Attitude from GPS Measurements on One Antenna. *NASA Tech Brief*, June 1998.

[16] Ebinuma, T. *Precision Spacecraft Rendezvous Using Global Positioning System: An Integrated Hardware Approach*. PhD thesis, The University of Texas at Austin, Austin, TX, August 2001.

[17] Ely, Todd A. Mars Network Radiometric Measurement Models and Data Interfaces for the Electra and CE-505 Radios. November 2005.

[18] Escoubet, C.P., Schmidt, R., and Goldstein, M.L. CLUSTER - Science and Mission Overview. *Space Science Reviews*, Vol. 79:pp. 11–32, 1997.

[19] Ferguson, P., and J. How. Decentralized Estimation Algorithms for Formation Flying Spacecraft. In *Proceedings of the AIAA Guidance, Navigation, and Control Conference*, Austin, TX, August 2003.

[20] Ferguson, P., C. Park, M. Tillerson, and J. How. New Formation Flying Testbed for Analyzing Distributed Estimation and Control Architectures.

In *Proceedings of the AIAA Guidance, Navigation, and Control Conference*, Monterey, CA, August 2002.

[21] Folta, D., K. Hartman, K. Howell, and B. Marchand. Formation Control of the MAXIM L_2 Libration Orbit Mission. In *Proceedings of the AIAA/AAS Astrodynamics Specialist Conference and Exhibit*, Providence, RI, August 2004.

[22] Gill, E., M. Steckling, and P. Butz. GEMINI: A Milestone towards Autonomous Formation Flying. In *Proceedings of the ESA Workshop on On-Board Autonomy*, Noordwijk, October 2001.

[23] Hofmann-Wellenhoff, B., et al. *Global Positioning System Theory and Practice*. Springer Wien, New York, 1997.

[24] How, J.P., and M. Tillerson. Analysis of the Impact of Sensor Noise on Formation Flying Control. In *Proceedings of the American Control Conference*, pages pp. 3986–3991, June 2001.

[25] Kaplan, E., ed. *Understanding GPS Principles and Applications*. Artech House, Boston, 1996.

[26] Kitts, C., R. Twiggs, F. Pranajaya, J. Townsend, and B. Palmintier. Experiments in Distributed Microsatellite Space Systems. In *Proceedings of the AIAA Space Technology Conference and Exhibit*, Albuquerque, NM, September 1999.

[27] Kovach, K. New User Equivalent Range Error (UERE) budget for the Modernized Global Positioning System (GPS). *Proceedings of the ION National Technical Meeting*, pages pp. 550–573, January 2000.

[28] Lau, K., et al. An Innovative Deep Space Application of GPS Technology for Formation Flying Spacecraft. *Presented at the AIAA GNC Conference*, July 1996.

[29] Leitner, J. Formation Flying - The Future of Remote Sensing from Space. 2000.

[30] Madsen, J.D. *Robust Spacecraft Attitude Determination Using Global Positioning System Receivers.* PhD thesis, The University of Texas at Austin, May 2003.

[31] Martin-Mur, T., and Garcia-Martinez, C. Data Analysis of Space Based Relative GPS Experiments. *FDS-98*, AAS 98-325, 1998.

[32] Misra, P., and P. Enge. *Global Positioning System: Signals, Measurements, and Performance.* Number ISBN 0-9709544-1-7. Ganga-Jamuna Press, Lincoln, MA, 2nd edition edition, 2006.

[33] Moreau, M., et al. GPS Receiver Architecture and Expected Performance for Autonomous GPS Navigation in Highly Eccentric Orbits. *Journal of The Institute of Navigation*, Vol. 47(No. 3), Fall 2000.

[34] Moreau, M.C., E.P. Davis, J.R. Carpenter, D. Kelbel, G.W. Davis, and P. Axelrad. Results from the GPS Flight Experiment on the High Earth Orbit

AMSAT OSCAR-40 Spacecraft. In *Proceedings of the ION GPS Conference*, Portland, OR, September 2002.

[35] Mortimer, K., ed. NASA - ST5. *http://www.nasa.gov/mission_pages/st-5/main*, June 2006.

[36] Naasz, B., et al. Hardware-in-the-Loop Testing of Continuous Control Algorithms for a Precision Formation Flying Demonstration Mission. 2000.

[37] Parkinson, B.W., and J.J. Spilker. *Global Positioning System: Theory and Applications*, volume Vol. 1. American Institute of Aeronautics and Astronautics, 1996.

[38] Purcell, G. Autonomous Formation Flyer (AFF) Sensor Technology Development. *TMO Progress Report 42-134*, August 1998.

[39] Robertson, A., T. Corazzini, and J.P. How. Formation Sensing and Control Technologies for a Separated Spacecraft Interferometer. In *Proceedings of the American Control Conference*, Philadelphia, PA, June 1998.

[40] Stewart, S., and G. Holt. "Real-Time Attitude Determination of a Nanosatellite Using GPS Signal-to-Noise Ratio Observations,". *Presented at the 19th AIAA/USU Conference on Small Satellites*, August 2005.

[41] Szebehely, V., and H. Mark. *Adventures in Celestial Mechanics*. John Wiley and Sons, New York, 2nd ed. edition, 1998.

[42] Tapley, B.D., B.E. Schutz, and G.H. Born. *Statistical Orbit Determination*. Elsevier Academic Press, Burlington, MA, 2004.

[43] Tapley, B.D., S. Bettadpur, M. Watkins, and C. Reigber. The Gravity Recovery and Climate Experiment: Mission Overview and Early Results. *Geophysical Research Letters*, Vol. 31(LO9607), 2004.

[44] Tillerson, M., et al. Distributed Coordination and Control of Formation Flying Spacecraft. In *Proceedings of the American Control Conference*, pages pp. 1740–1745, 2003.

[45] Vallado, David A. *Fundamentals of Astrodynamics and Applications*. Microcosm Press, El Segundo, CA, 2nd ed. edition, 2001.

[46] Wertz, J.R., and W.J. Larson, editor. *Space Mission Analysis and Design*. Microcosm Press, El Segundo, CA, 3rd ed. edition, 1999.

[47] Wu, B., V. Chu, P. Chen, and T. Ting. FORMOSAT-3/COSMIC Science Mission Update. *GPS Solutions*, Vol. 9:pp. 111–121, June 2005.

[48] Yim, J.R., J.L. Crassidis, and J.L. Junkins. Autonomous Orbit Navigation of Two Spacecraft System Using Relative Line of Sight Vector Measurements. In *Proceedings of the 14th AIAA/AAS Spaceflight Mechanics Meeting*, number AAS 04-257, pages 2447–2460, February 2004.

Vita

Greg Nate Holt was born in Austin, Texas in 1978, the son of Nate and Nancy Holt. He attended Hyde Park Baptist High School, graduating as valedictorian of the class of 1996. From there, he attended the University of Texas at Austin to study Aerospace Engineering. While still an undergraduate he worked as a research assistant for Dr. Steve Nerem on the Lunar Prospector impact project. In 2000 he received his Bachelor of Science degree, graduating with highest honors. Greg then enrolled as a graduate student in Aerospace Engineering at UT under Dr. E. Glenn Lightsey. In 2002, he received a Master of Science in Engineering degree with a thesis titled "Benchmark Testing for Spaceborne Global Positioning System Receivers." Greg then became program manager of the FASTRAC (Formation Autonomy Spacecraft with Thrust, Relnav, Attitude, and Crosslink) nanosatellite project at UT. He stepped down as program manager in 2004 to become the GPS/Navigation lead and helped develop the multi-purpose sensor for the spacecraft.

Permanent address: 5401 Bull Run Circle
Austin, Texas 78727

This dissertation was typeset with LaTeX[†] by the author.

[†] LaTeX is a document preparation system developed by Leslie Lamport as a special version of Donald Knuth's TeX Program.